

# Future Glacial Lake Outburst Flood (GLOF) hazard of the South Lhonak Lake, Sikkim Himalaya



Ashim Sattar <sup>a,e,\*</sup>, Ajanta Goswami <sup>b</sup>, Anil.V. Kulkarni <sup>c</sup>, Adam Emmer <sup>d</sup>, Umesh K. Haritashya <sup>a</sup>, Simon Allen <sup>e,f</sup>, Holger Frey <sup>e</sup>, Christian Huggel <sup>e</sup>

<sup>a</sup> Department of Geology and Environmental Geosciences, University of Dayton, Dayton, OH, USA

<sup>b</sup> Department of Earth Sciences, Indian Institute of Technology, Roorkee, India

<sup>c</sup> Divecha Centre for Climate Change, Indian Institute of Science, Bangalore, India

<sup>d</sup> Cascade – Mountain Processes and Mountain Hazards Group, Institute of Geography and Regional Science, University of Graz, Austria

<sup>e</sup> Environment and Climate: Impacts, Risks and Adaptation (ECLIM), Department of Geography, University of Zurich, Switzerland

<sup>f</sup> Climatic Change Impacts and Risks in the Anthropocene (C-CIA), Institute for Environmental Sciences, University of Geneva, Geneva, Switzerland

## ARTICLE INFO

### Article history:

Received 12 September 2020

Received in revised form 2 March 2021

Accepted 13 May 2021

Available online 17 May 2021

### Keywords:

Glacial lake outburst flood  
South Lhonak  
Himalaya  
Hazard  
Risk  
Uncertainty

## ABSTRACT

The Teesta basin in Sikkim Himalaya hosts numerous glacial lakes in the high altitude glacierized region, including one of the largest and the fastest-growing South Lhonak Lake. While these lakes are mainly located in remote and unsettled mountain valleys, far-reaching glacial lake outburst floods (GLOFs) may claim lives and damage assets up to tens of kilometers downstream. Therefore, evaluating GLOF hazard associated with current and potential future glacier-retreat-driven changes is of high importance. In this work, we assess the future GLOF hazard of the South Lhonak Lake by integrating glacier and hydrodynamic modeling to calculate the lake's future volume and hydraulic GLOF characteristics and impacts along the valley. We identify the increased susceptibility of the lake to potential avalanche impacts as the lake grows in the future. Here we model six avalanche scenarios of varying magnitudes to evaluate the impact-wave generated in the lake and overtopping flow at the dam. Avalanche simulations indicate that the frontal moraine is susceptible to overtopping. The overtopping flow hydraulics is evaluated along the channel assuming no erosion of the moraine. Further, we consider three lake-breach scenarios to model GLOFs originating from the lake, flow propagation, and its downstream impacts. The uncertainty in the breach parameters including breach width and time of failure are calculated to estimate the upper and the lower hydraulic limits of potential future GLOF events. Further, the uncertainty in the flow hydraulics was evaluated using dynamic flood routing of six GLOFs that originate from the lake. Hydrodynamic GLOF modeling resulted in a predicted peak discharge of  $4311 \text{ m}^3 \text{s}^{-1}$ ,  $8000 \text{ m}^3 \text{s}^{-1}$ , and  $12,487 \text{ m}^3 \text{s}^{-1}$  for breach depths of 20 m, 30 m, and 40 m respectively. The large-potential scenario suggests that maximum flow depth and flow velocity at Chungthang, a town proximally located to a major hydropower station built-in 2015, could reach up to 25–30 m and  $6\text{--}9 \text{ m s}^{-1}$ , respectively. Mapping infrastructure exposed to GLOFs in the Teesta valley shows that many settlements and assets located along the river channel at Chungthang are potentially exposed to future GLOFs, indicating the need to conduct a full environmental impact assessment and potentially undertake GLOF risk mitigation measures.

© 2021 The Author(s). Published by Elsevier B.V. This is an open access article under the CC BY-NC-ND license (<http://creativecommons.org/licenses/by-nc-nd/4.0/>).

## 1. Introduction

The formation of glacial lakes can be seen as a direct indication of glacier changes, as most of these lakes form when glaciers retreat (Gardelle et al., 2011; Zhang et al., 2015). In the High Mountain Asia, glacier mass loss and recession is observed in most parts except for regions in the Karakoram and Kunlun (Bolch et al., 2012; Azam et al., 2018; King

et al., 2019; Farinotti et al., 2020). With increased glacier retreat, there has been an accelerated lake growth over the past few decades in high mountains of the world (Hoelzle et al., 2003; Paul et al., 2004; Gardelle et al., 2011; Bolch et al., 2012; Haritashya et al., 2018; Shugar et al., 2020). This growth of the proglacial lakes depends on the exposed bed topography as glaciers retreat (Linsbauer et al., 2016; Allen et al., 2016; Sattar et al., 2019b; Emmer et al., 2021). As the lake grows, so does its potential to cause catastrophic Glacial Lake Outburst Floods (GLOF) depending on factors including the total drainable volume, exposure to potential mass-movement impacts, and structural integrity of the frontal moraine (in the case of moraine-dammed lakes). In

\* Corresponding author at: Environment and Climate: Impacts, Risks and Adaptation (ECLIM), Department of Geography, University of Zurich, Switzerland.

E-mail addresses: [ashim.sattar@gmail.com](mailto:ashim.sattar@gmail.com), [ashim.sattar@geo.uzh.ch](mailto:ashim.sattar@geo.uzh.ch) (A. Sattar).

Himalaya, expansion of the existing lakes and the formation of numerous new glacial lakes are occurring rapidly (Komori, 2008; Watanabe et al., 2009; Gardelle et al., 2011; Raj and Kumar, 2016; Shukla et al., 2018; Haritashya et al., 2018; Shugar et al., 2020). Many of these lakes are dammed by unconsolidated glacial deposits forming unstable moraines, failure of which can be triggered by various mechanisms, but commonly from mass movements that enter into the lake, for example, avalanches, rockfalls, landslides, and calving processes (Richardson and Reynolds, 2000; Liu et al., 2013). GLOFs can also be triggered by extreme meteorological conditions, especially heavy rainfall events that cause degradation of the damming moraine and leads to overfilling of the lake (Worni et al., 2012). The Kedarnath disaster in the central Himalaya is one of the most devastating examples (Allen et al., 2016). Owing to the recent developments in terms of infrastructure and human settlements within the mountainous regions of the Himalaya, the existence of glacial lakes in the high altitude of the Himalaya has become a major concern to the downstream communities (Richardson and Reynolds, 2000; Bajracharya et al., 2008; Worni et al., 2013; Sattar et al., 2019a; Sattar et al., 2019c).

Catastrophic GLOFs have been reported from the Hindu Kush–Karakoram–Himalaya (HKKH) region, Cordillera Blanca, Andes, Rocky Mountains, Swiss Alps, and many other glacierized mountain ranges, causing severe damage to humankind and infrastructure (e.g., Anacona et al., 2015; Somos-Valenzuela et al., 2016; Allen et al., 2016; Ray et al., 2016; Emmer, 2018; Veh et al., 2019). For example, Dig Tsho glacial lake in the Mt. Everest region of Nepal Himalaya produced a GLOF in 1985 that killed five people and destroyed a hydropower station (Vuichard and Zimmermann, 1987). The 2013 Kedarnath disaster (central Himalaya), which was a GLOF from Chorabari Lake associated with flash-flooding and landslides triggered by intense precipitation in the region, led to over 6000 fatalities and washed away the major part of a settlement located just over 1 km downstream of the lake (Allen et al., 2016). Similarly, a GLOF from Lake Palcacocha in Peruvian Cordillera Blanca claimed at least 1600 lives and wiped out one-third of Huaraz city in 1941 (Carey et al., 2012; Hugel et al., 2020). The risk that a potentially dangerous lake may present to the low-lying areas can be unrecognized unless a detailed hazard assessment is undertaken. Therefore, evaluating the characteristics of a glacial lake, its surroundings, and local hydrodynamical flood modeling allow us to understand how a valley will behave in case of a potential GLOF event. Therefore, a detailed hazard assessment of the existing dangerous lakes is necessary for disaster preparedness and mitigation.

GLOFs in Himalaya have attracted the attention of scientists as well as practitioners over the years. Recent studies on hazard assessment of the glacial lakes in the Indian Himalayan region revealed numerous lakes that can produce future GLOFs and cause downstream damage (Worni et al., 2013; Dubey and Goyal, 2020). Worni et al. (2013) presented a glacial lake inventory covering most of the Indian Himalaya. The lakes were mapped using Landsat ETM+ of 2000 to 2002 and Google Earth imageries. A total of 251 glacial lakes with an area  $> 0.01 \text{ km}^2$  were identified, of which 12 lakes were identified as critical and 93 as potentially critical based on a lake outburst probability analysis and considering potential downstream exposure. A recent study evaluated the potential downstream impact of 329 lakes across the Indian Himalaya, showing that 36 lakes are exposed to potential avalanche impact-zones (Dubey and Goyal, 2020). However, detailed case studies focusing on the future GLOF hazard potential of the critical glacial lakes in the Himalaya are still quite limited.

For Sikkim Himalaya, numerous glacial lake inventories and statewide hazard assessments are available (Mool et al., 2003; Raj et al., 2013; Worni et al., 2013; Aggarwal et al., 2017; Sattar et al., 2019a). Mool et al. (2003) presented the first glacial lake inventory, where 266 lakes were mapped with a total area of  $20.2 \text{ km}^2$ , of which 14 lakes were identified to be potentially critical. Another glacial lake inventory reported 14 potentially dangerous lakes out of 320 total lakes

mapped (Raj et al., 2013). Later, Aggarwal et al. (2017) presented an inventory using Resourcesat-2 and LISS IV imageries, reporting a total of 472 lakes ( $> 0.01 \text{ km}^2$ ), of which 21 lakes were identified as potentially critical. Strikingly, in all these studies, South Lhonak Lake has been identified as potentially dangerous with a high outburst probability.

In Sikkim, the lake-terminating glaciers have shown accelerated growth compared to the glaciers with no lakes (Aggarwal et al., 2017). South Lhonak glacier is no different; it is one of the fastest retreating glaciers and the associated proglacial lake has become the largest and fastest-growing in the state (Aggarwal et al., 2017). The glacier receded  $\sim 2 \text{ km}$  in 46 years from 1962 to 2008 (Raj et al., 2013). It further retreated by  $\sim 400 \text{ m}$  from 2008 to 2019 (Fig. 1). It has been a growing concern now about the hazard potential of this lake, as the downstream valley is heavily populated with numerous settlements and infrastructure. The Central Water Commission, Government of India, initiated an advisory to evaluate the South Lhonak glacier and its lake system. The initial hazard assessment of the South Lhonak Lake based on the current condition suggests that the lake has great potential to significantly impact the downstream region (Sattar et al., 2019a). However, as the lake grows, it becomes important to evaluate both current and future hazards and the risk it imposes on the downstream region.

This study focuses on evaluating the future GLOF hazard of the South Lhonak Lake considering a series of potential GLOF scenarios. Our specific objectives include (i) mapping the maximum extent and calculating the future lake volume; (ii) identification of potential avalanche source zones and modeling impact of avalanches on the lake; (iii) characterization of the avalanche-triggered impulse-wave and overtopping; (iv) future GLOF-hazard assessment using moraine-breach modeling and flood routing; (v) uncertainty assessment of GLOF hydraulics using hydrodynamic modeling; and (vi) mapping infrastructure at GLOF risk along the valley.

## 2. Study area and its importance

The lake-terminating South Lhonak glacier and its proglacial lake ( $27^{\circ}54'20''\text{N}$  and  $88^{\circ}10'20''\text{E}$ ) is located at an elevation of 5200 m a.s.l. in the Teesta Basin, Sikkim, Himalaya (Fig. 1A & B). The glacier has a total area of  $12.5 \text{ km}^2$ , as mapped in 2019. During the past 29 years, the length of the glacier reduced from 6.4 km to 5.1 km, while the overall glacier shrank by  $\sim 0.96 \text{ km}^2$  (Fig. 1 D-G). In line with the glacier retreat, the lake has been exhibiting significant growth over the years as it grew from  $0.42 \text{ km}^2$  in 1990 to  $1.35 \text{ km}^2$  in 2019 (Fig. 1D-G). The frontal moraine damming the lake has a width of approximately 500 m and it gets narrow towards the north, where a surface outflow from the lake is located. The surficial outflow channel cuts the moraine dam in the north-northeast direction while the main valley is oriented towards the east (see Fig. 1). The crest height of the frontal part of the damming moraine (south from the outflow channel) is 7 m above lake level, as measured in the field by Sharma et al. (2018). This part of the moraine is characterized by a hummocky surface indicating the presence of ice within the dam with several small lakes on the moraine surface (thermokarst of precipitation-filled), and the absence of vegetational cover.

So far, there has not been any reported GLOF; however, Kumar and Murugesh Prabhu (2012) presented a report to the Government of Sikkim, where the lake outlet is stated to show evidence of a previous GLOF (Fig. 1C). Bathymetric measurements indicate a current lake volume of  $65.8 \times 10^6 \text{ m}^3$ , with a maximum depth of 131 m (Sharma et al., 2018). The lakes' narrow outlet drains into the Goma channel, which joins the Zemu River 36 km downstream of the lake. It further joins the Lachen River at Hema located 40 km downstream. The valley downstream of the lake is moderately populated, with a major town being Chungthang located 62 km downstream of the lake where the Teesta Stage III hydropower dam is located. According to the 2011 census report ([censusindia.gov.in](http://censusindia.gov.in)), Chungthang had more than 10,000 inhabitants, living in more than

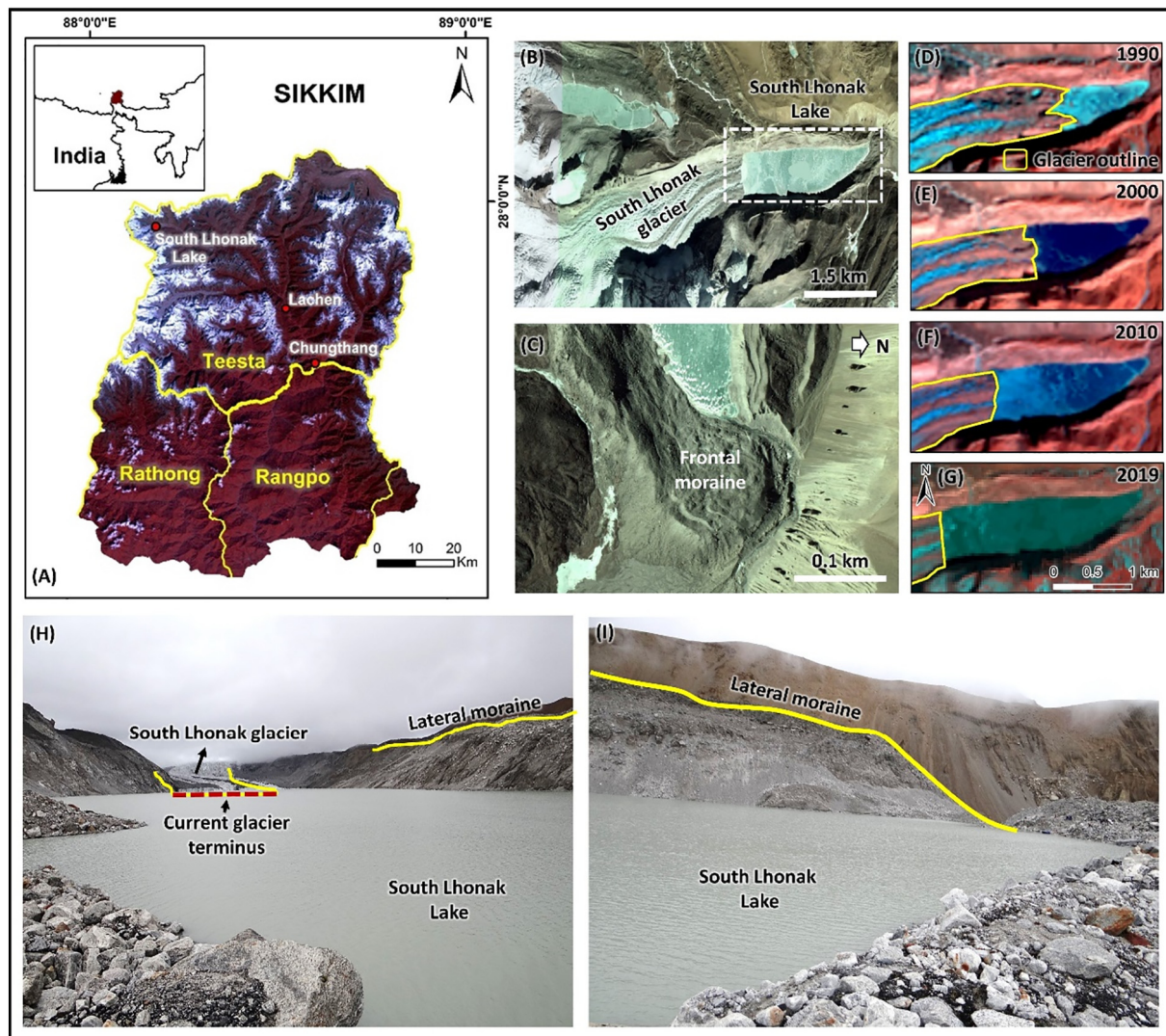


**Fig. 1.** (A) Map of the Indian state of Sikkim showing the location of the South Lhonak Lake and the two major settlements along the valley; Google Earth image showing the bird-eye view of (B) the tongue of the South Lhonak glacier and its associated proglacial lake; and (C) frontal moraine damming the South Lhonak Lake; (D–G) Landsat image showing the evolution of the lake as the glacier retreated from 1990 to 2019; (H–I) Field photograph of the South Lhonak Lake showing the current glacier terminus, lateral moraines, and frontal part of the moraine (photo courtesy: Department of Science and Technology, Government of Sikkim).

1900 households. The town has evolved over the years and has especially seen rapid growth after the construction of a hydropower station in 2015. Other small townships like Lachen, Latong, and Yuigang exist along the flow channel.

### 3. Data used and methods

#### 3.1. Data used

The present study utilizes glacier outlines available in the Randolph Glacier Inventory (RGI), an open-source database for the existing glaciers in the globe (<http://www.glims.org/RGI>). The latest available version of the glacier boundary for the year 2000 (RGI 6.0) is used as a base to map the South Lhonak glacier. Cloud-free (<10%) Landsat-5 images for the years 1990, 2000, 2010, and Landsat-8 for 2019 available at (<https://earthexplorer.usgs.gov/>) were used for temporal mapping of the glacier and the proglacial lake. The Shuttle Radar Topography Mission (SRTM) Digital Elevation Model (DEM) with a spatial resolution of 30 m (for ice-thickness modeling) and ensemble ice-thickness product (Farinotti et al., 2019) were used to derive spatially distributed glacier-bed maps. We use SRTM DEM (available globally for the year 2000) to calculate the ice-thickness using the GlabTop model (Linsbauer et al., 2012) and

compared it with ensemble ice-thickness from Farinotti et al. (2019), which is available for the 2000 glacier extent. We also compare the various ice-thickness outputs (GlabTop and ensemble) by comparing it to the field bathymetry (measured in the year 2014–16) for the portion where the glacier retreated thereby exposing the bedrock and leading to the growth of the lake (see Fig. 5). This enabled validating the ice-thickness that we use to calculate the future volume of the lake. We used field-based lake bathymetry (Sharma et al., 2018) and the modeled overdeepening to derive the lake's future volume. To extract terrain elevation for hydrodynamic GLOF modeling, we used the Advanced Land Observing Satellite (ALOS) – Phased Array type L-band Synthetic Aperture Radar (PALSAR) DEM with a spatial resolution of 12.5 m (Source DEM 30m SRTM resampled to 12.5m). It is a radiometrically terrain-corrected elevation product with global coverage released in October 2014 by the Alaskan Satellite Facility (<https://asf.alaska.edu/data-sets/derived-data-sets/los-palsar-rtc/los-palsar-radiometric-terrain-correction/>). Channel roughness (Manning's N) is obtained in a spatially distributed manner along the flow-path using GlobCover (v2.3). GlobCover is a globally validated LULC product, acquired by MERIS on-board of Envisat (Bicheron et al., 2008). This is cross-verified using high-resolution geo-referenced CNES/Airbus imagery tiles of Google Earth. Table-S1 (supplementary) lists the details of the datasets used.

### 3.2. Lake growth and its future extent/volume

RGI outlines were slightly modified to map the glacier, and to derive ice-thickness and glacier terminus changes. The lake boundary for each year (1990, 2000, 2010, and 2019) is manually digitized. The future volume is derived by combining the current bathymetry-based volume and the volume of the frontal overdeepening. For that, the glacier bed of the South Lhonak glacier is mapped using spatially distributed glacier ice-thickness approaches.

We used a shear-stress based method to reconstruct glacier ice-thickness, which is dependent on the relationship between basal stress and the slope of the glacier (GlabTop, c.f., Linsbauer et al., 2012). In a comprehensive assessment of modeled glacier-ice thickness outputs derived using different numerical approaches, Farinotti et al. (2017) concluded that the most reliable ice-thickness estimates could be derived by averaging the ice-thickness outputs from multiple models. Therefore, in the present study, we compare the South Lhonak glacier-bed derived using GlabTop for different values of  $f$  (Linsbauer et al., 2012) and the ensemble ice-thickness (Farinotti et al., 2019) with the field-measured lake bathymetry. The ensemble ice-thickness is a distributed ice-thickness product derived by averaging the spatially distributed ice-thickness solution from four different models (i.e., Huss and Farinotti, 2012; Frey et al., 2014; Fürst et al., 2017; and Maussion et al., 2018). The glacier bed is obtained by GIS-based spatial arithmetic operation considering glacier surface elevation and ice-thickness distribution, given as  $B_E = S_E - H$ , where  $B_E$  is the spatially distributed glacier-bed elevation (m a.s.l.),  $S_E$  is the glacier-surface elevation (m a.s.l.), and  $H$  is the ice-thickness (m). The different modeled glacier bed outputs were compared to field-collected bathymetry (Sharma et al., 2018) across two cross-sectional profiles (e.g., Fig. 4I and J). The output with the lowest Root Mean Square Error (RMSE) was further considered to calculate the extent and volume of the future lake (e.g., Fig. 5). The future lake volume is calculated by combining the volume of the

overdeepened site ( $V_{ovd}$ ) and the present-lake bathymetric volume ( $V_{lake}$ ). The schematic of a proglacial lake system and its future growth is shown in Fig. 2. The flowchart (Fig. 3) summarizes the entire methodology adopted in the study.

### 3.3. Identification of potential future GLOF triggers, avalanche modeling, and overtopping

Here, we overlay the South Lhonak Lake's future extent (as mapped in Section 3.2) to identify mass movement zones from where an avalanche can enter the lake and potentially trigger a future GLOF event. Preliminarily, we consider a slope threshold of  $>30^\circ$  to identify the surrounding avalanche-prone slopes, and we calculate the topographic potential of the surrounding slopes for mass movements into the lake. The concept of topographic potential assumes an impact into a lake is possible from any slope  $> 30^\circ$ , from which the overall slope trajectory to the lake is  $>14^\circ$  ( $\tan\alpha = 0.25$ ) (see Allen et al., 2019). These conservative values are based on typical ice and/or rock avalanches reported globally, although mass movements from more gentle slopes and obtaining larger runout distances are possible in exceptional cases.

We further model avalanches using the debris flow module within Rapid Mass Movement Simulation (RAMMS) software. RAMMS is based on the Voellmy-Salm method that solves the shallow water equation in two-dimension (Christen et al., 2010). We used ALOS PALSAR DEM as terrain input for simulation. We define an avalanche release area for the mass-movement susceptible slopes, calculated based on the topographic potential. Other input parameters for the model include debris density, Coulomb friction ( $\mu$ ), and turbulent friction ( $\xi$ ) (Bartelt et al., 1999). We consider values of 0.12 and  $1000 \text{ m s}^{-2}$  for  $\mu$  and  $\xi$ , respectively. We note that constraining the friction parameters needs further calibration and validation. However, the sensitivity analysis of these values indicates that they are conservative and the accepted standard values produce the fastest, farthest traveling, and densest avalanches (Bartelt et al., 2013; Lala

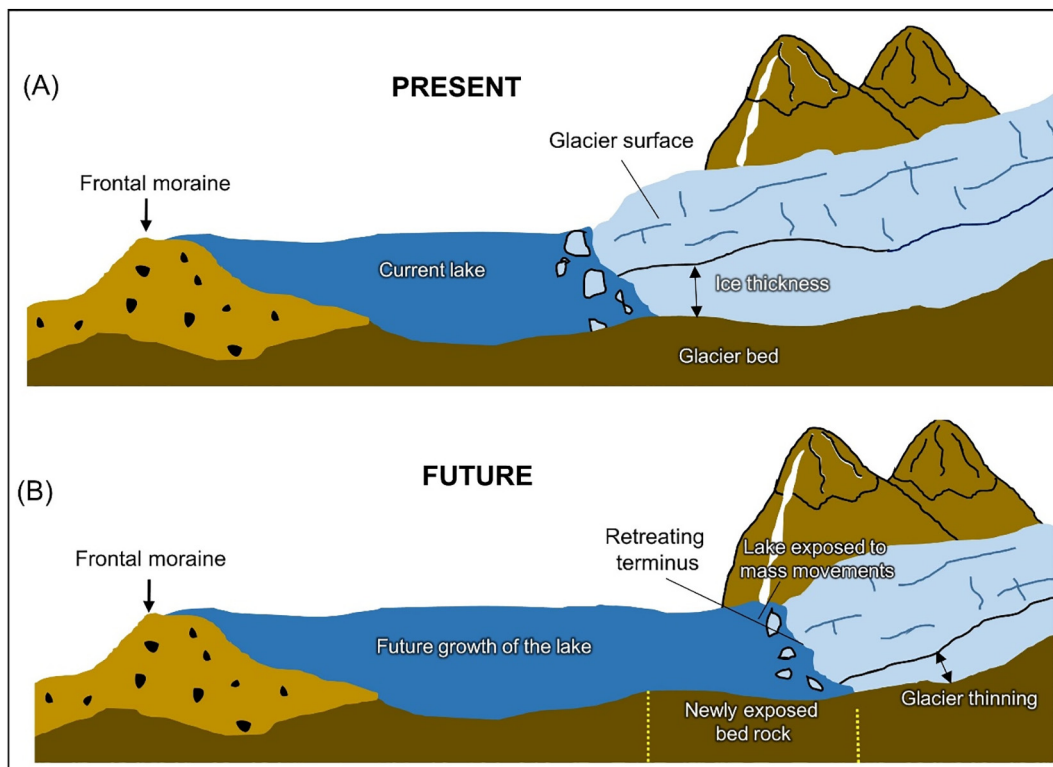


**Fig. 2.** Schematic diagram showing (A) a proglacial lake system at present; (B) lake grows as the overdeepened glacier bed is exposed in the future by glacier retreat, further exposing it to potential mass movements that can enter the lake.

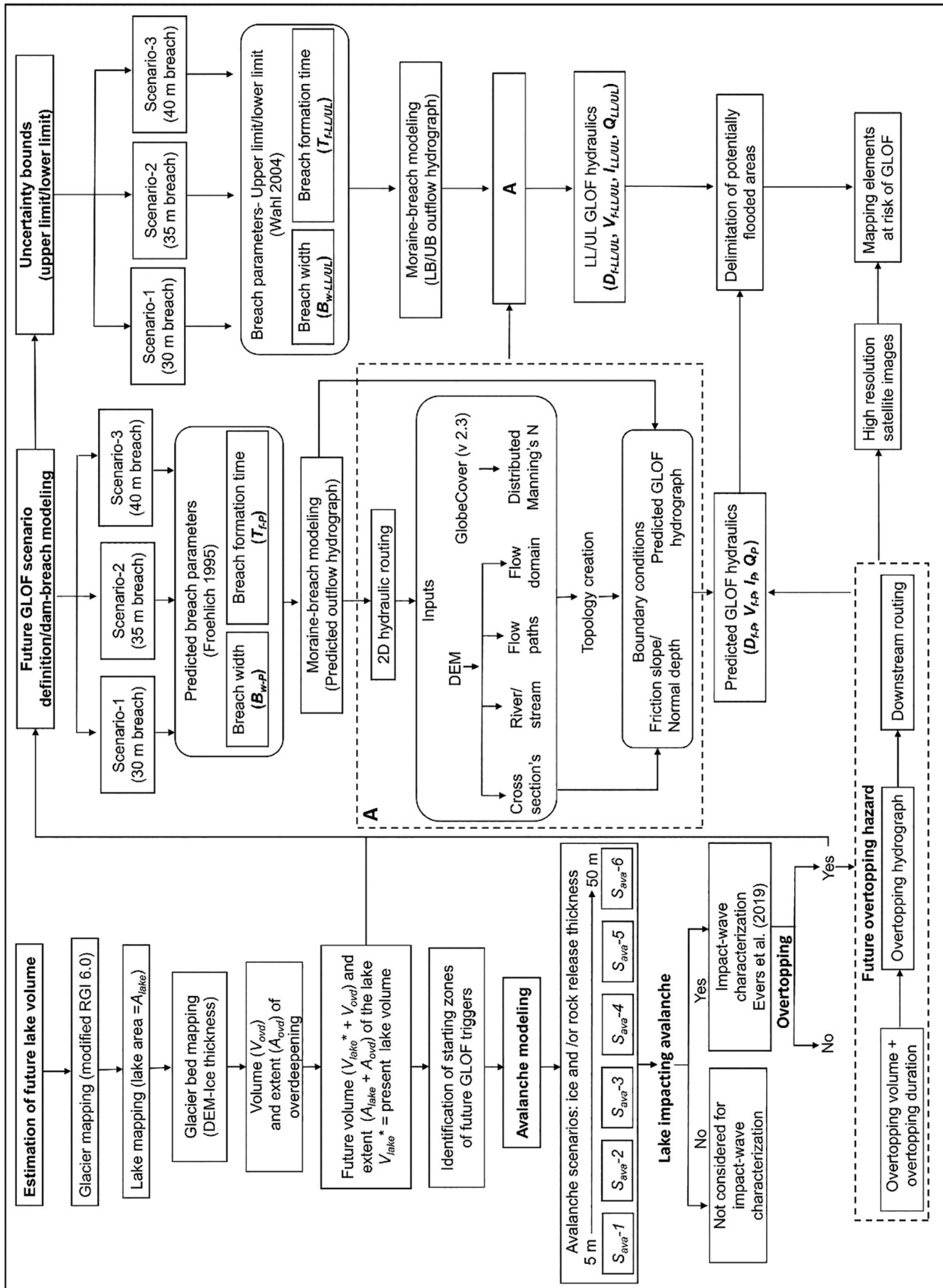


Fig. 3. Flowchart of the entire methodology.

et al., 2018). We assume these values for modeling potential avalanches in the South Lhonak glacier valley as these values were previously used to model avalanches in glacier-covered terrains in the Himalaya (Somos-Valenzuela et al., 2016; Lala et al., 2018). The input parameters also agree with other studies globally where similar values were used to model ice and/or rock avalanches (Sosio et al., 2008; Schneider et al., 2010; Schneider et al., 2014; Frey et al., 2018). In the present study, we model six avalanche scenarios, keeping the release area constant but with varying thicknesses of the detaching mass. We consider two low-magnitude scenarios ( $S_{ava-1}$  and  $S_{ava-2}$ ), where we assume an ice and/or rock thickness of 5 m and 10 m at the source for  $S_{ava-1}$  and  $S_{ava-2}$  respectively. For moderate-magnitude avalanches, we increase the thickness to 20 m ( $S_{ava-3}$ ) and 30 m ( $S_{ava-4}$ ). Further, we model two high-magnitude avalanches with ice and/or rock thickness of 40 m ( $S_{ava-5}$ ) and 50 m ( $S_{ava-6}$ ). These assumed scenarios are similar to previously modeled avalanches in the Himalaya (Rounce et al., 2016; Lala et al., 2018), and generally align to the range of thicknesses typically considered for such steep cliff situations (Huggel et al., 2004). The corresponding release volume was calculated based on the ice and/or rock thickness and area of the release zone.

Further, we model the impulse wave generated by each of the above avalanche impacts on the lake using the Evers et al. (2019) model, a revised version of the earlier model (Heller et al., 2009), with incorporated up-to-date studies. We calculate the run-up and overtopping at the dam if an initial impulse-wave is caused by any of the avalanche scenarios ( $S_{ava-1}$  to  $S_{ava-6}$ ). This empirical approach has been widely used for avalanche-induced impulse-wave characterization in glacial lakes in the Himalaya (Lala et al., 2018; Byers et al., 2019; Byers et al., 2020). The latest Evers et al. (2019) model computes the characteristics of an avalanche-induced impulse-wave originating from the site of the impact that propagates towards the damming moraine and eventually overtops. It further computes the characteristics of wave run-up and overtopping at the damming site. The model requires avalanche characteristics and morphological dimensions of the lake, as inputs. We compute avalanche characteristics like impact volume (in  $\text{m}^3$ ), impact velocity ( $V_s$ , in  $\text{m s}^{-1}$ ), slide width ( $S_w$ , in m), impact ice and/or rock-thickness (in m), run-up angle ( $\beta$ ), and impact angle ( $\alpha$ ) of the main flow direction of the avalanche compared to the longitudinal axis of the lake. Here the total impact volume is calculated for the ice and/or rock that enters the lake during a potential avalanche (Fig. 7H). The bulk density of the avalanche material is considered as  $1000 \text{ kg m}^{-3}$  assuming it to be a mixture of ice and/or rock, similar to other Himalayan studies (Somos-Valenzuela et al., 2016; Lala et al., 2018). Morphological characteristics like freeboard, dam-crest height above the lake level, dam-crest width, distance of the impact from the frontal moraine, and still-water depth at the impact site were calculated based on modeled bathymetry, field information (Sharma et al., 2018), and high resolution Google earth imagery. We empirically model the impulse wave to evaluate its characteristics like overtopping wave-height, overtopping-velocity, and volume at the dam site. Further, we calculate the overflow hydrographs in case of overtopping, which are used for two-dimensional downstream flood routing using HEC-RAS (version 5.0.7; <https://www.hec.usace.army.mil/software-/hec-ras/>). Here we do not consider any erosion dynamics of the frontal moraine. The downstream flow hydraulics, including flow depth ( $D_f$ ), flow velocity ( $V_f$ ), and inundation ( $I_f$ ) of the waves with different overtopping volumes are evaluated along the flow channel. For flood-routing simulations, the terrain conditions are kept constant as that of the dam-breach simulations described below (see Section 3.4.1).

### 3.4. GLOF modeling and routing

#### 3.4.1. GLOF scenarios

We note that overtopping or overfill of a lake can exert shear stress that can exceed the strength of the moraine (Korup and Tweed, 2007; Westoby et al., 2014). Therefore, evaluating dam-breach hazards becomes important. Here, apart from the overtopping hazard of the lake, we also

evaluate the lake-breach hazard considering a series of breach events originating from the lake. We assume different scenarios with varied breach dimensions of the frontal moraine and evaluate its GLOF hydraulics. We use the HEC-RAS hydrodynamic model to simulate potential moraine-breach events of the lake. This hydrodynamic tool has been previously used to model outbursts from other glacial lakes (Klimeš et al., 2016; Kougkoulos et al., 2018; Sattar et al., 2019a, 2019c; Sattar et al., 2020). The initial dam geometry (dam-crest, side slopes, width, and freeboard) of the lake is extracted using DEM, high-resolution Google Earth imagery, and published values of the moraine characteristics (Sharma et al., 2018).

Based on the future lake bathymetry and potential release volume, here we evaluate three dam-breach scenarios- (i) Scenario-1 ( $SC-1_P$ ; subscript "P" stands for "predicted"), low-potential GLOF with a breach depth ( $h_{b1}$ ) of 20 m, (ii) Scenario-2 ( $SC-2_P$ ), moderate-potential GLOF with breach depth ( $h_{b2}$ ) of 30 m, and (iii) Scenario-3 ( $SC-3_P$ ), large-potential GLOF with breach depth of 40 m ( $h_{b3}$ ) (Fig. 5B). Most documented past-GLOF events in the Himalaya did not lead to the lake's complete drainage (Zheng et al., 2021), so for South Lhonak Lake, we assume similar scenarios where potential breach ceases at a maximum depth of 40 m in the moraine, i.e., full removal of the downstream slope of the dam up to 40 m (Fujita et al., 2013). This is based on the potential flood volume (PFV), which is a function of the total breach depth ( $h_b$ ). Considering a large-potential scenario is important for hazard mitigation and preparedness. The corresponding flood release-volume in each case is calculated based on future bathymetry (as calculated in Section 3.2).

Dam-break simulation requires information on the breach parameters including breach width ( $B_w$ ) and time of breach formation ( $T_f$ ) as inputs. Several empirical approaches are available to calculate these parameters. Wahl (2004) presented a comprehensive assessment of the different empirical methods and reported that Froehlich (1995a, 1995b) has the lowest prediction-uncertainty and is globally used to model glacial lake outbursts (for e.g. Osti and Egashira, 2009; Wang et al., 2012; Anacona et al., 2015; Wang et al., 2018; Majeed et al., 2021). Therefore it is used here to calculate the predicted breach width ( $B_{w-P}$ ) and time of breach formation ( $T_{f-P}$ ) for each scenario (Eqs. (1) and (2)) (Table 2). Considering the preconditions of the South Lhonak Lake including the surrounding avalanche-prone slopes, future lake extent, and the anticipated most likely future GLOF triggers (avalanches that enter into the lake), we model overtopping failure of the frontal moraine in each of the moraine-breach scenarios ( $SC-1_P$ ,  $SC-2_P$ , and  $SC-3_P$ ). The output is obtained in the form of a discharge/outflow hydrograph (discharge vs. time) that varies based on the total volume released and the breach parameters. The predicted outflow peak-discharge ( $Q_{-P}$ ) is compared to the empirically calculated discharge (Eq. (3), Froehlich, 1995b).

$$B_{w-P} = 0.1803 K_o (V_w)^{0.32} (h_b)^{0.19} \quad (1)$$

$$T_{f-P} = 0.00254 (V_w)^{0.53} (h_b)^{-0.9} \quad (2)$$

$$Q_{-P} = 0.607 V_w^{0.295} h_w^{1.24} \quad (3)$$

The outflow hydrographs obtained for each scenario are dynamically routed as unsteady flow to evaluate the flow hydraulics downstream of the lake using HEC-RAS (2D). We assess the GLOF hydraulics including  $D_f$ ,  $V_f$ , and  $I_f$  along the flow channel from the lake to the Chungthang town. The upstream and downstream boundary conditions were set as the modeled GLOF-outflow hydrograph and normal depth, respectively. A distributed Manning's N along the main flow-channel is considered for hydraulic GLOF-routing. The LULC (GlobeCover v2.3) is extracted for a buffer of 500 m along the main flow channel, from the lake to "Chungthang". The LULC is dominated by vegetation in the lower part of the flow area from 40 km downstream of the lake (Sattar et al., 2019a). This can have a significant impact on the downstream flow hydraulics. Therefore, we considered a distributed channel roughness to evaluate the effect of LULC on the potential GLOF flow. The

roughness value along the flow channel ranged between 0.034 and 0.11, with higher values representing vegetation.

### 3.4.2. Uncertainty analysis (lower and upper GLOF limits)

In hydrodynamic GLOF routing, the boundary conditions control the flow hydraulics along a given channel (Westoby et al., 2014). In GLOF prediction, the outflow breach-hydrograph, which is a function of the breach parameters ( $B_{w-P}$  and  $T_{f-P}$ ), is considered the upstream boundary. Here, we note that predicted breach parameters can be associated with some degree of uncertainty. Therefore, we empirically calculate the uncertainty bounds (lower and upper) of each breach parameter ( $B_{w-P}$  and  $T_{f-P}$ ) for each scenario (SC-1<sub>P</sub>, SC-2<sub>P</sub>, and SC-3<sub>P</sub>) (Wahl, 2004). Since no model is currently available to our knowledge that determines the breach uncertainty of glacial-lake dams, we employ Wahl (2004), which applies to embankment dams composed of earth materials (Wan and Fell, 2004). This model has been previously used to assess the uncertainty in the breach parameters of glacial lake in the Himalaya (Somos-Valenzuela et al., 2015). Further, we determine the lower and the upper uncertainty in the flow hydraulics along the given channel as described below. Here, the terms Lower Limit (LL) and Upper Limit (UL) define the lower-bound uncertainty and the upper-bound uncertainty to the predicted GLOF hydraulics which are calculated using Eqs. (4) and (5) (Wahl, 2004).

$$LL = P \left( 10^{-e-2Se} \right) \quad (4)$$

$$UL = P \left( 10^{-e+2Se} \right) \quad (5)$$

where  $P$  is the predicted breach parameters ( $B_{w-P}$ ,  $T_{f-P}$ ), and predicted discharge ( $Q_P$ ),  $e$  and  $2Se$  are mean prediction error and width of uncertainty band, respectively, that are derived using regression in a log-log space of documented dam-break cases (Wahl, 1998; Wahl, 2004). Here,  $e$  and  $2Se$  has a value of 0.01 and  $\pm 0.39$  for  $B_w$ , based on the regression (Froehlich,

1995a vs. observed) of 70–80 documented dam-break cases. Similarly,  $e$  and  $2Se$  has a value of  $-0.22$  and  $\pm 0.64$  for  $T_f$  based on the regression (Froehlich, 1995a vs. observed) of 30–40 dam-break cases. For  $Q$ , 30–40 test cases were considered for regression (Froehlich, 1995b vs. observed), where  $e$  and  $2Se$  have calculated values of  $-0.04$  and  $\pm 0.32$ , respectively. To evaluate the uncertainty in the GLOF hydraulics in a given flow, we initially calculate the lower and the upper limit of the breach parameters ( $B_{w-LL/UL}$  and  $T_{f-LL/UL}$ ) and the discharge range ( $Q_{range}$ ) for each potential GLOF scenario (SC-1<sub>P</sub>, SC-2<sub>P</sub>, and SC-3<sub>P</sub>) (Table 2). This is followed by dam-break modeling to calculate the outflow discharge hydrograph. Here, we obtain six outflow hydrographs (i.e., two for each scenario) based on the calculated LL and UL of the breach parameters ( $B_{w-LL/UL}$  and  $T_{f-LL/UL}$ ) with their peak discharge ( $Q_{LL/UL}$ ). The outflow hydrographs modeled for each scenario (SC-1<sub>LL/UL</sub>, SC-2<sub>LL/UL</sub>, and SC-3<sub>LL/UL</sub>) are hydrodynamically routed to evaluate the uncertainty in downstream hydraulics. The downstream boundary conditions and terrain in the model setup are kept constant as that in Section 3.4.1. The overall methodology is summarized in Fig. 3.

### 3.5. Mapping GLOF hazard intensity and infrastructures at risk of GLOF

We used the flow parameters like  $V_f$  and  $D_f$  to define the hazard intensity downstream of the lake for different predicted GLOF scenarios (SC-1<sub>P</sub>, SC-2<sub>P</sub>, and SC-3<sub>P</sub>). The hazard zones were defined based on combined thresholds of  $V_f$  and  $D_f$  (Fig. 13). The thresholds are based on the recent international guidelines on glacier and permafrost hazard assessment (GAPHAZ, 2017). Further, we used shapefiles of flood inundation extent for each predicted GLOF scenario and high-resolution satellite images from Google Earth (taken in 2019) to manually map at-risk downstream infrastructures between South Lhonak Lake and Chunthang town. We mapped three categories of infrastructures: (i) bridges, (ii) buildings (mainly houses), and (iii) industry and mining areas.

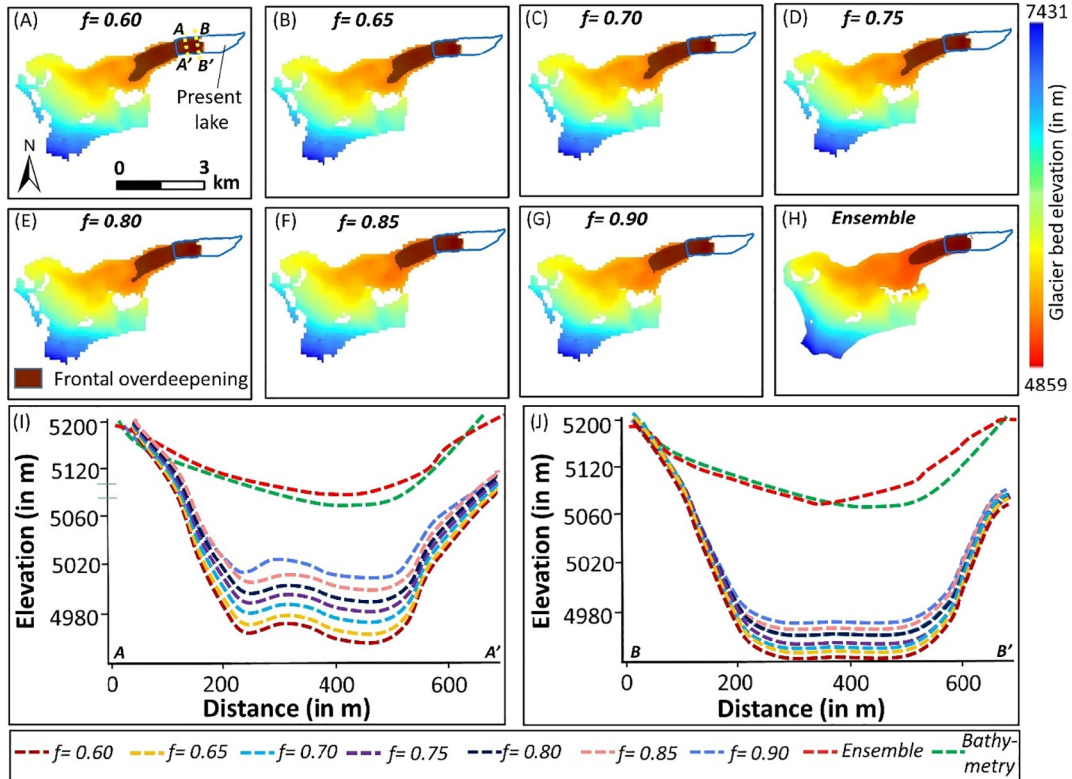


**Fig. 4.** Spatially distributed modeled glacier bed for different values of ' $f$ ' using GlabTop (A-G); Ensemble (H) (Farinotti et al., 2019); (I-J) cross-sectional profiles of glacier beds along AA' and BB'.

## 4. Results

### 4.1. Future lake extent and volume

The glacier bed calculated using GlabTop (Fig. 4A-G) and ensemble ice-thickness (Fig. 4H) were compared along two cross-sections of the South Lhonak Lake bathymetry. We note that the performance of ice-thickness models may vary from glacier to glacier (Farinotti et al., 2017). Also, for shear stress-based models like GlabTop, it becomes difficult to determine the value of  $f$  as it is dependent on the general form of the glacier cross-sections, and longitudinal and transverse stresses, which may vary within a glacier (Linsbauer et al., 2012). The GlabTop-derived bathymetry showed an overestimation of the lake depths with a calculated RMSE of 51 m ( $f = 0.9$ ) (Fig. 4). The calculated RMSE for lower values of  $f$  (0.85–0.6) resulted in comparatively higher RMSE ranging between 65 m to 80 m (Fig. 4A-F). The spatial extent of the overdeepening reduces with an increase of  $f$ , and so does the depth. All the GlabTop estimates resulted in overestimating the depth values (Fig. 4I-J). However, based on the sensitivity of ice thickness to  $f$  (Fig. 4), the RMSE will further reduce with higher values of  $f$ , which we do not consider for this study rather we focus on the range from 0.6 to 0.9 (Paterson 1994). The future lake depths were very well represented in the glacier bed with an RMSE of 5 m, when derived using the ‘Ensemble’ ice-thickness which is based on the law of averages (Farinotti et al., 2019). This was further considered to calculate the volume of the frontal overdeepening, which has a maximum depth of 92 m and a total area of 0.6 km<sup>2</sup>. The total future volume of the South Lhonak Lake was calculated by combining the present lake volume (Sharma et al., 2018) and the modeled volume of the overdeepening (Fig. 5). The total volume of the future lake was calculated to be  $114.8 \times 10^6$  m<sup>3</sup>, with a total area of 1.86 km<sup>2</sup>, representing an overall increase in lake volume of 74.4% relative to today. The future lake extends upstream up to 1.2 km from the current terminus.

### 4.2. Impact wave characterization and overtopping

The identified avalanche-prone cliffs based on the mass movement potential (Fig. 6A) exhibit lateral crevasses as evidence of downslope movement. At a distance of ~930 m upstream of the current terminus, one such heavily crevassed surface over a steep cliff can be identified

(Fig. 6B) and appears to be the most immediate threat to the lake at this point.

Avalanche modeling shows that the low-magnitude avalanches ( $S_{ava-1}$  and  $S_{ava-2}$ ) terminate before reaching the future lake, and are hence, no threat (Fig. 7A-B). The released volumes were  $5.2 \times 10^5$  m<sup>3</sup> and  $9.1 \times 10^5$  m<sup>3</sup> for  $S_{ava-1}$  and  $S_{ava-2}$ , respectively. The moderate-magnitude scenarios ( $S_{ava-3}$  and  $S_{ava-4}$ ) with a release volume of  $2.0 \times 10^6$  m<sup>3</sup> and  $3.2 \times 10^6$  m<sup>3</sup> reaches the lake. Similarly, for the high-magnitude avalanches ( $S_{ava-5}$  and  $S_{ava-6}$ ), the release volumes were calculated as  $4.1 \times 10^6$  m<sup>3</sup> and  $5.2 \times 10^6$  m<sup>3</sup>, respectively. These avalanches have a high potential impact on the lake, with higher runout distances than moderate-magnitude avalanches. We calculated the volume of avalanche mass that entered the lake in the cases of scenarios  $S_{ava-2}$  to  $S_{ava-6}$ . The total avalanche volume that enters the lake at its posterior end (Fig. 7C-F) ranged from  $4.0 \times 10^5$  m<sup>3</sup> to  $2.1 \times 10^6$  m<sup>3</sup>. The impact velocity ( $V_s$ ) at the site of impact ranged from  $24.8 \text{ m s}^{-1}$  to  $37.2 \text{ m s}^{-1}$  (Fig. 7G). The slide width ( $S_w$ ) is the width of the avalanche during impact and is considered to be the width of the lake, i.e., 450 m in this of South Lhonak Lake. The impact angle ( $\alpha$ ) along the direction of avalanche flow is calculated from the DEM and is equal to the trajectory slope, which is 25°. The still water depth of the lake at the impact site is derived from the modeled future-bathymetry and is estimated as 45 m. The above parameters were used as input to the Evers et al. (2019) impulse-wave model to calculate the wave-crest amplitude ( $a$ ) and wave height ( $H$ ) at the source (impact site). Further, we use these values to model the run-up and characterize the overtopping wave. For that, the run-up angle ( $\beta$ ) is calculated, as the slope of the moraine facing the lake. The crest height of 7 m above lake level was considered based on the field measured value of the frontal moraine (Sharma et al., 2018). The overtopping depth ( $D_{ovr}$ ) and velocity ( $V_{ovr}$ ) for the lake-impacting avalanches ( $S_{ava-2}$  to  $S_{ava-6}$ ) ranged from 2.5 m to 6.7 m and  $10.6 \text{ m s}^{-1}$  to  $20.7 \text{ m s}^{-1}$  respectively (Fig. 7I). The total overtopping volume ranged between  $1.8 \times 10^4$  m<sup>3</sup> (for  $S_{ava-2}$ ) to  $4.8 \times 10^5$  m<sup>3</sup> (for  $S_{ava-6}$ ). The characteristics of individual avalanches and the resulting overtopping are given in Table 1.

The overtopping hydrographs calculated for each impact scenario ( $S_{ava-2}$  to  $S_{ava-6}$ ) based on the overtopping volume and duration resulted in peaks ranging from  $1825 \text{ m}^3 \text{s}^{-1}$  to  $4850 \text{ m}^3 \text{s}^{-1}$  (see Supplementary Fig. S1). The hydraulic routing of the overtopping hydrograph with the highest peak ( $S_{ava-6}$ ) resulted in  $D_f$  and  $V_f$  reaching up to 3 m

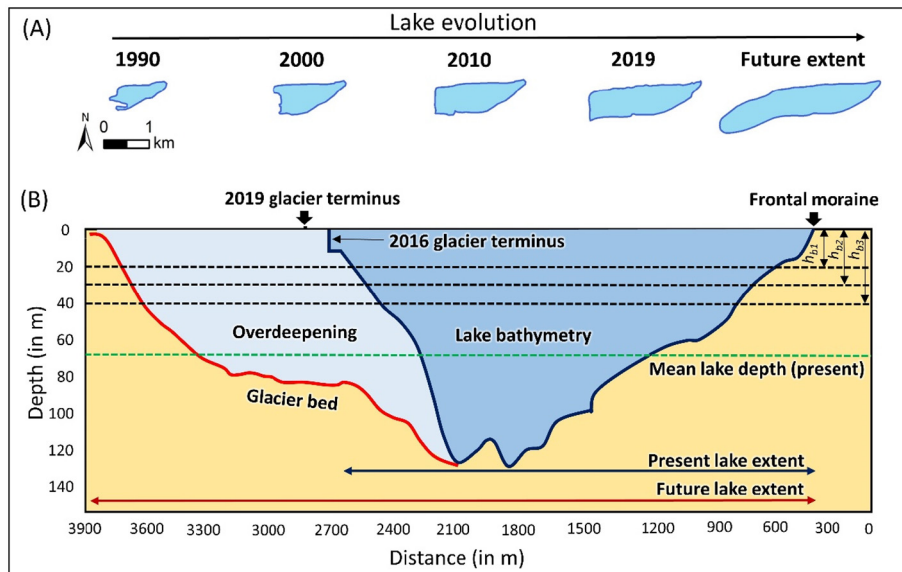


**Fig. 5.** (A) Evolution of the South Lhonak Lake from 1990 to 2019 and the modeled future (maximum) extent of the lake; (B) Cross-sectional profile of the lake along the central axis, showing the current lake bathymetry (Sharma et al., 2018) and the overdeepening; marked are the breach depths of the three potential GLOF events modeled in this study ( $h_{b1}$ ,  $h_{b2}$ , and  $h_{b3}$ ).

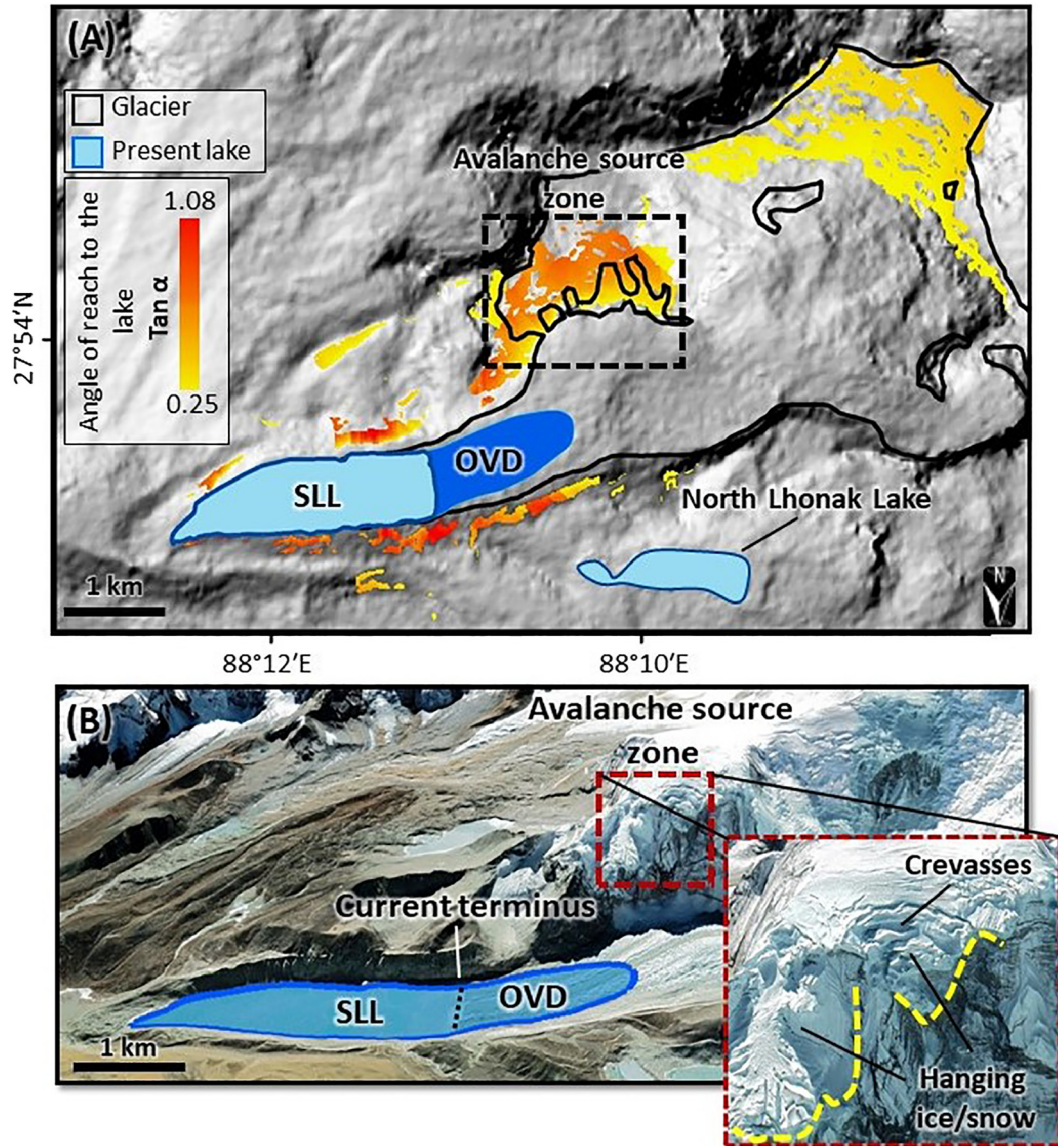


**Fig. 6.** (A) South Lhonak glacier-lake system showing the extent of the present lake (SLL) and overdeepening (OVD); the topographic potential for mass movements is shown for the surrounding slopes; (B) avalanche source zone showing highly crevassed and hanging ice and/or rock (located ~930 m upstream of the current terminus).

and  $21 \text{ ms}^{-1}$ , respectively (Fig. 8). Due to relatively flat terrain just in front of the lake, there is a significant loss in the momentum of the flow and it terminates at a distance of 13 km downstream of the lake, i.e., 33 km upstream of Lachen. The  $D_f$ ,  $V_f$ , and runout distances for the other overtopping scenarios ( $S_{ava}-2$  to  $S_{ava}-5$ ) are less than  $S_{ava}-6$ .

#### 4.3. Outburst flood hydraulics

Modeling results for the avalanche-induced impact wave indicates that the frontal moraine of the South Lhonak Lake is susceptible to overtopping, with a possibility of initiating moraine breaching processes. From a physical process point of view, overtopping waves could trigger a dam breach process, but observational evidence indicates that this occurs rarely. Moraine dam breach processes are more commonly related to a slow or sudden rise of the lake level and the associated increase in discharge at the outflow where shear stresses increase to a level where erosion is initiated and progressively increases to dam failure (Worni et al., 2012). In this case, it is a large influx of avalanche material that impacts the lake (Section 4.2). However, other causes can be because of failure of the North Lhonak Lake located

upstream, or temporary blockage of the outlet, for instance by snow or ice, that could result in a rise of lake level.

We relied on scenario-based modeling to appropriately analyze the dam breach and downstream propagation, considering three breaching scenarios of the frontal moraine with a maximum breach of 40 m (Table 2). In Scenario-1, the predicted low-potential GLOF ( $SC-1_p$ ) produced a GLOF peak of  $\sim 4300 \text{ m}^3 \text{s}^{-1}$ . We evaluated flow hydraulics at two cross-sections located downstream of the lake at 46 km (Lachen) and 62 km (Chunghthang). At Lachen,  $SC-1_p$  arrives at 210 min after the initiation of the breach producing a peak discharge of  $\sim 3320 \text{ m}^3 \text{s}^{-1}$ . Further downstream at Chunghthang, the GLOF arrives at 448 min after the breach event with a peak of  $1134 \text{ m}^3 \text{s}^{-1}$ . Here, predicted  $D_f$  and  $V_f$  reaches up to 10–13 m and  $3\text{--}5 \text{ m s}^{-1}$ , respectively (Fig. 10 and Fig. 11). In Scenario-2, the predicted moderate-potential GLOF ( $SC-2_p$ ) produced a GLOF peak of  $8000 \text{ m}^3 \text{s}^{-1}$ . At Chunghthang, GLOF arrives 114 min earlier than  $SC-1_p$ , where  $D_f$  and  $V_f$  increase by  $\sim 2 \text{ m}$  and  $\sim 2 \text{ m s}^{-1}$ , respectively, compared to the low-potential GLOF. The large-potential Scenario-3 ( $SC-3_p$ ) reaches Chunghthang 218 min and 104 min earlier than  $SC-1_p$  and  $SC-2_p$ , respectively. It produces a GLOF peak of  $6420 \text{ m}^3 \text{s}^{-1}$  with  $D_f$  reaching up to 23–30 m and  $V_f$  up to

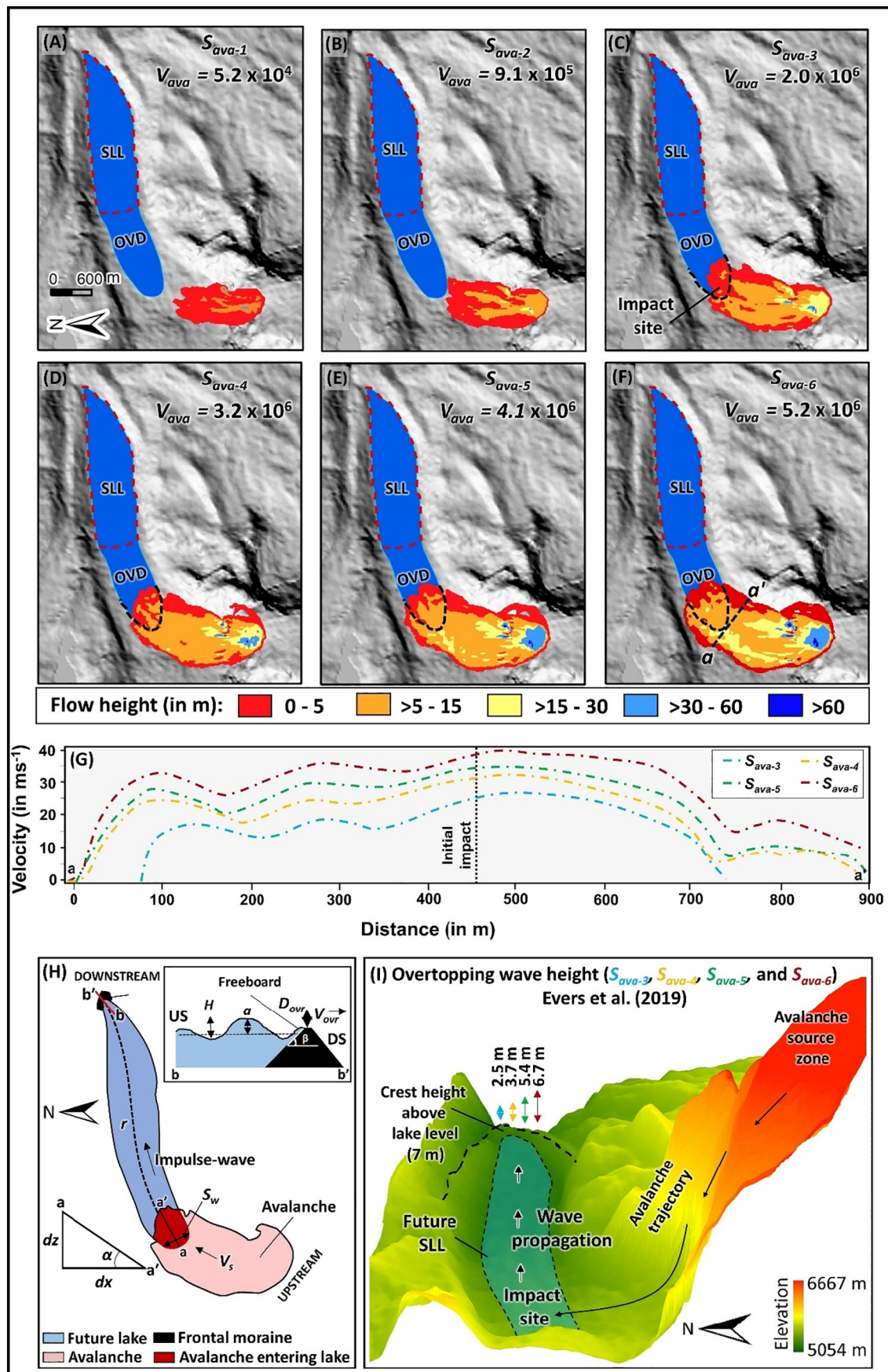


**Fig. 7.** (A-F) Modeled avalanche scenarios for different released volumes; the present extent of the South Lhonak Lake is shown as SLL and the overdeepening as OVD; (G) Avalanche velocity profile along aa' (see panel F for profile location); (H) Avalanche parameters for impulse-wave modeling (Evers et al., 2019); (I) 3D view showing the avalanche source zone, trajectory, and overtopping wave heights of the impulse-wave.

**Table 1**

Avalanche and impact wave characteristics.

Avalanche characteristics					Overtopping wave characteristics				
Avalanche	Release volume ( $\times 10^6 \text{ m}^3$ )	Maximum impact velocity ( $\text{m s}^{-1}$ )	Maximum impact thickness (m)	Volume entering the lake ( $\times 10^5 \text{ m}^3$ )	Overtopping height (m)	Overtopping volume ( $\times 10^4 \text{ m}^3$ )	Overtopping duration (s)	Overtopping peak discharge ( $\text{m}^3 \text{s}^{-1}$ )	GLOF termination (km)
$S_{\text{ava}-1}$	0.05								
$S_{\text{ava}-2}$	0.9								
$S_{\text{ava}-3}$	2.0	24.8	7.8	4.0	2.5	1.8	19.5	1825	6.5
$S_{\text{ava}-4}$	3.2	30.0	13.6	4.2	3.7	2.6	20.1	2625	8
$S_{\text{ava}-5}$	4.1	34.4	14.5	15.6	5.4	3.9	20.5	3925	11
$S_{\text{ava}-6}$	5.2	37.2	17.3	21.1	6.7	4.8	21.0	4850	13

10–15  $\text{m s}^{-1}$ . Fig. 10 shows the inundation boundaries and spatially distributed plots of flow depth and flow velocity at Chungthang, for each predicted GLOF scenario.

#### 4.4. Uncertainty in GLOF hydraulics

The uncertainty in the breach parameters calculated for LL and UL for each scenario (Section 3.4.2) is reflected in the GLOF peaks ( $Q_{\max}$ ) (Table 2) and flow hydraulics (Fig. 9 and Fig. 11). The time to reach the peak discharge ( $T_{\text{peak}}$ ) and the arrival time downstream ( $T_{\text{arr}}$ ) was greatly influenced by the LL and UL of the GLOF parameters ( $B_w$  and  $T_f$ ) (Fig. 9). In dam-break simulations, the outflow hydrograph is more sensitive to  $T_f$  compared to  $B_w$  (Singh and Snorrason, 1982; Basheer et al., 2017; Sattar et al., 2020). In the lower limit, where the  $B_w$  and  $T_f$  are lower than the predicted values, the  $Q_{\max}$  is reached earlier and vice versa.

In Scenario-1, the uncertainty in the GLOF  $Q_{\max}$  ranges between 2321 and 4311  $\text{m}^3 \text{s}^{-1}$ . The maximum uncertainty in the time taken to reach the peak ( $T_{\max}$ ) is 94 min (Fig. 9). Routed hydrographs at Chungthang show uncertainty in the GLOF arrival time ( $T_{\text{arr}}$ ) of 82 min and uncertainty in  $Q_{\max}$  ranges between 907 and 1134  $\text{m}^3 \text{s}^{-1}$ . Here, the uncertainty in  $D_f$  and  $V_f$  is calculated to be in the range of 16 to 18 m and 2 to 3  $\text{m s}^{-1}$  respectively (Fig. 11). In Scenario-2, an uncertainty in GLOF  $Q_{\max}$  ranges between 4202 and 8000  $\text{m}^3 \text{s}^{-1}$ . The uncertainty in  $T_{\max}$  is 142 min. At Chungthang, an uncertainty of  $T_{\text{arr}}$  is calculated to be 104 min, and uncertainty in  $Q_{\max}$  ranges between 1370 and 1670  $\text{m}^3 \text{s}^{-1}$ . The uncertainty in  $D_f$  and  $V_f$  is calculated to be in the range of 16 to 17.5 m and 1.9 to 3.4  $\text{m s}^{-1}$ , respectively. Similarly, in Scenario-3, the uncertainty in the GLOF  $Q_{\max}$  ranges between 7140 and 12,487  $\text{m}^3 \text{s}^{-1}$ . The uncertainty in routed  $Q_{\max}$  at Chungthang ranges between 4776 and 6422  $\text{m}^3 \text{s}^{-1}$ . Here, the uncertainty in  $D_f$  and  $V_f$  is

calculated to be in the range of 21 to 24 m and 2.8 to 4  $\text{m s}^{-1}$ . Note that the uncertainty in  $D_f$  and  $V_f$  is measured for a single point at Chungthang (see Fig. 10 for location and Fig. 11 for plots).

#### 4.5. Infrastructures at risk of flooding

The number of infrastructure objects at risk of flooding differs among modeled GLOF scenarios. It ranges from 183 for scenario  $SC_{1P}$  (includes 5 bridges, 176 houses, and 2 industrial facilities) to 266 for  $SC_{3P}$  (includes 13 bridges, 248 houses, and 5 industrial facilities) (Fig. 12). Most of these are located in Chungthang, the town that experienced rapid urbanization during the past few years due to new construction and operation of the hydropower station. Additional sites that could be flooded are located a few km upstream of Chungthang (Fig. 12). Hazard intensity mapping based on thresholds of GLOF hydraulics (Fig. 13) shows that most of the settlements situated along the flow channel at Chungthang are within moderate to high GLOF intensity zones in a low-potential ( $SC_{1-P}$ ) and moderate-potential ( $SC_{3-P}$ ) GLOF scenarios. In the large-potential GLOF scenario ( $SC_{3-P}$ ), these settlements fall under high-intensity zones (Fig. 13). We note that in Chungthang where the hydropower dam is located, the water surface is reflected in the DEM used for the study. Therefore, we calculate the flow parameters like flow depth and flow velocity considering the water surface as the base for the flow. For hazard mapping at Chungthang (settlement), which is located along the shoreline of the flowchannel we assume that any changes in the base flow would be negligible in comparison with the flow hydraulics generated by the outburst flood. However, we note that a detailed investigation of GLOF impacts on the hydropower dam, and possible backwash affecting Chungthang, would require more information about the depth and volume of the reservoir, including seasonal variations, which is beyond the scope of the study.

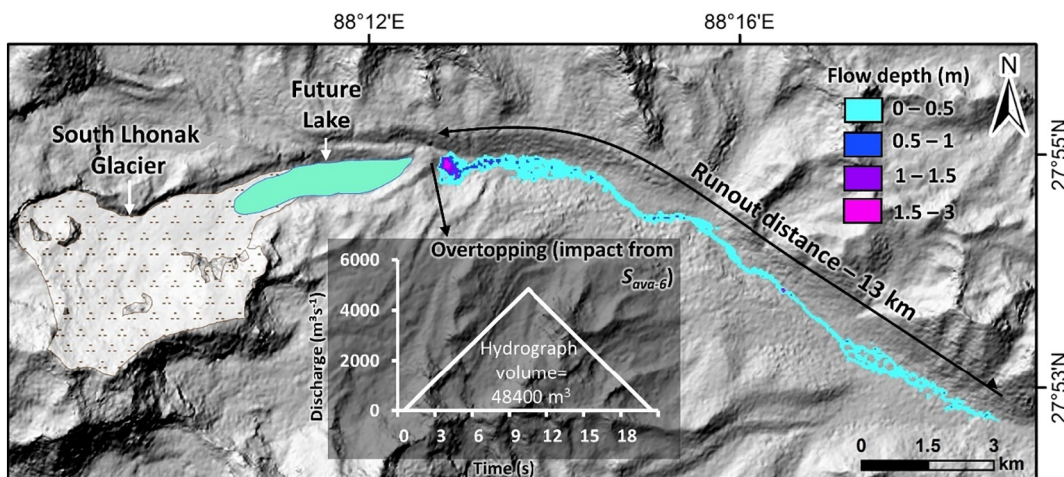


**Fig. 8.** Overtopping flow depth long the channel resulting from avalanche impact ( $S_{\text{ava}-6}$ ); the subset shows the overtopping hydrograph calculated based on impact wave from  $S_{\text{ava}-6}$ ; note that due to relatively flat terrain just in front of the lake, there is a significant loss in the momentum of the flow and the flow tends to slow down and terminates at 13 km downstream of the lake i.e. 33 km upstream of Lachen.

**Table 2**

Calculated breach parameters for each scenario - Predicted ( $P$ ), Lower Limit ( $LL$ ), and Upper Limit ( $UL$ ). Note that the predicted discharge is higher than the upper limits due to the higher breach formation time ( $T_f$ ).

Breach scenarios	Breach width ( $B_w$ ) (in m)			Breach formation time ( $T_f$ ) (in h)			Peak discharge ( $Q$ ) (in $\text{m}^3\text{s}^{-1}$ )			Peak discharge range ( $Q_{range}$ ) (in $\text{m}^3\text{s}^{-1}$ )	
	$P$	$LL$	$UL$	$P$	$LL$	$UL$	$P$	$LL$	$UL$		
SC-1 ( $h_{b1}$ )	20 m	119.4	47.5	286.4	1.8	0.7	12.9	4311	3367	2321	2263–9876
SC-2 ( $h_{b2}$ )	30 m	146.8	58.4	352.1	1.5	0.6	11.1	8000	6230	4202	4198–18,330
SC-3 ( $h_{b3}$ )	40 m	169.5	67.6	407.5	1.4	0.5	10.0	12,487	11,437	7140	6553–28,606

## 5. Discussion

### 5.1. Drivers of GLOF risk

One of the critical questions in glacier lake investigations worldwide is to understand how GLOF risk has evolved and how it will impact downstream in the future. Studies have shown that GLOF risk will likely increase in the future, considering the increase in number of new lakes, and increased triggering potential (Allen et al., 2016; Haeberli et al., 2016; Drenkhan et al., 2019). Also, the changing patterns of exposure are an equally important driver of GLOF risk (Hock et al., 2019). Although the number of GLOF studies has increased over recent years, only a few studies address more than one GLOF risk component, and consider past and/or future changes in these drivers (Emmer, 2018; Huggel et al., 2020). Therefore, our study took a holistic look at South Lhonak Lake and established multiple scenarios to understand the

GLOF potential and its possible impact. Specifically, our study includes future modeling of lake breach and understanding potential GLOF's impact on the rapidly increasing downstream infrastructures because of the new hydropower site at Chungthang (Fig. 14).

#### 5.1.1. Physical drivers of GLOF hazard

The width of the terminal moraine that dams the South Lhonak Lake is not uniform (Fig. 1C & I) and is thinning towards the ends. Hummocky surface of the dam indicates that it likely contains buried ice and be subject to future degradation. We note that the moraine's stability can change with time due to changes in the structural integrity (Clague and Evans, 2000; Richardson and Reynolds, 2000) due to melting of buried ice, impact waves that lead to overtopping flows, extreme meteorological conditions, such as, cloud burst quickly overfilling the lake and triggering progressive erosion of the dam, etc. Additionally, continuing

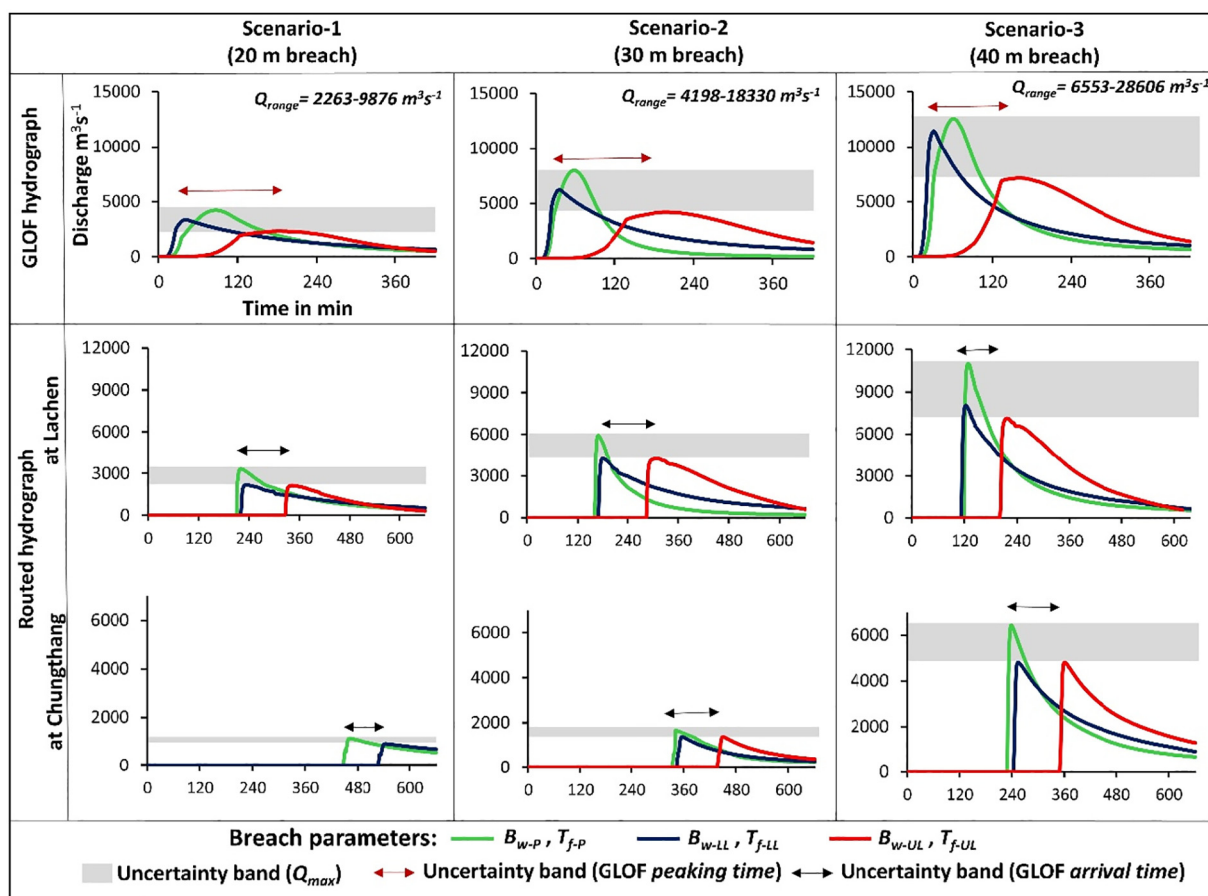


**Fig. 9.** GLOF hydrographs and routed hydrographs calculated from the Predicted, Lower Limit, and Upper Limit GLOF parameters; the grey boxes (shaded) and red arrows (two-sided) represent the uncertainty in peak discharge ( $Q_{max}$ ) and GLOF peak timing ( $T_{peak}$ ), respectively; black arrows (two-sided) represent the uncertainty in GLOF arrival timing ( $T_{arr}$ ). Routed hydrographs are along a cross-section at Lachen and Chungthang (see Fig. 1 for locations).

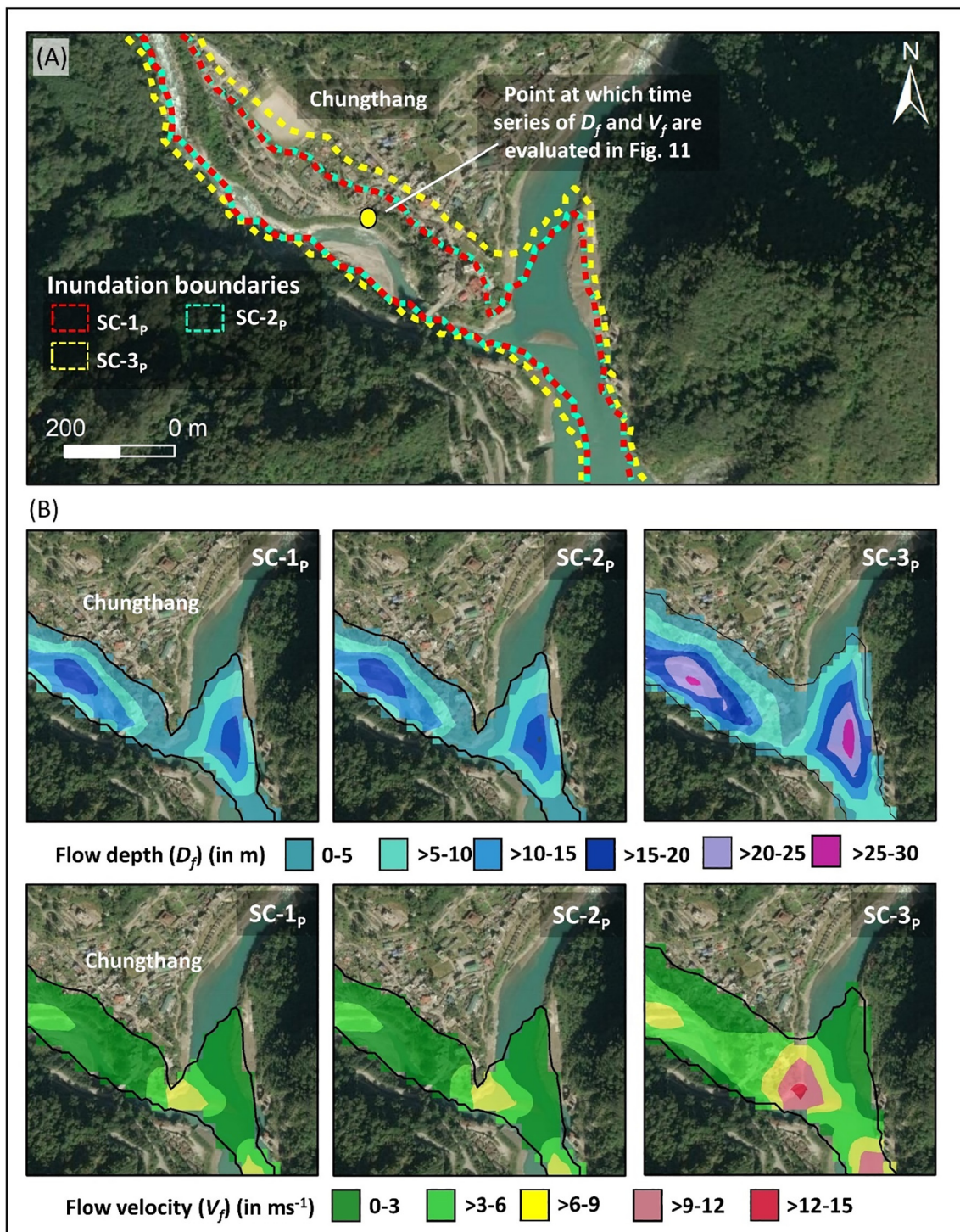


**Fig. 10.** (A) Inundation boundaries and (B) spatially distributed flow depth ( $D_f$ ) and flow velocity ( $V_f$ ) at Chungthang of each predicted GLOF scenario.

glacier retreat will bring the lake closer to steep and potentially degrading slopes (moraine, bedrock, and ice) (Haeberli et al., 2017).

Seismic activity can in principle also lead to degradation of the moraines' structural integrity, although not necessarily leading to an outburst (Kargel et al., 2016), and is an obvious trigger of large catastrophic ice/rock avalanches (Mergili et al., 2018a, 2018b). This is particularly concerning, as South Lhonak Lake is located in a highly active seismic zone and several earthquakes in the past had their epicenter in the vicinity of the lake. For example, the epicenter of 4.9 magnitude earthquake on Sept 19, 1991, and 6.9 magnitude on Sept 18, 2011, were located immediately behind Zemu glacier, 70 km south

of South Lhonak glacier ([USGS-earthquake.usgs.gov/earthquakes/eventpage/usp000j88b/](http://USGS-earthquake.usgs.gov/earthquakes/eventpage/usp000j88b/) executive). Although field evidence suggests that South Lhonak Lake is currently devoid of proximal slopes that can act as a primary source of an avalanche (Sharma et al., 2018), further consideration should be given to far-reaching rock/ice avalanches, particularly co-seismic events. Likewise, attention should be given to any tension cracks that may develop in proximal slopes as a result of lake expansion. In the current study, we have focused on a section of steep icy cliffs located 500 m upstream from the current terminus that can potentially be one of the zones that can fail and impact the lake (Fig. 6). Larger avalanche scenarios modeled here have proven sufficient to displace

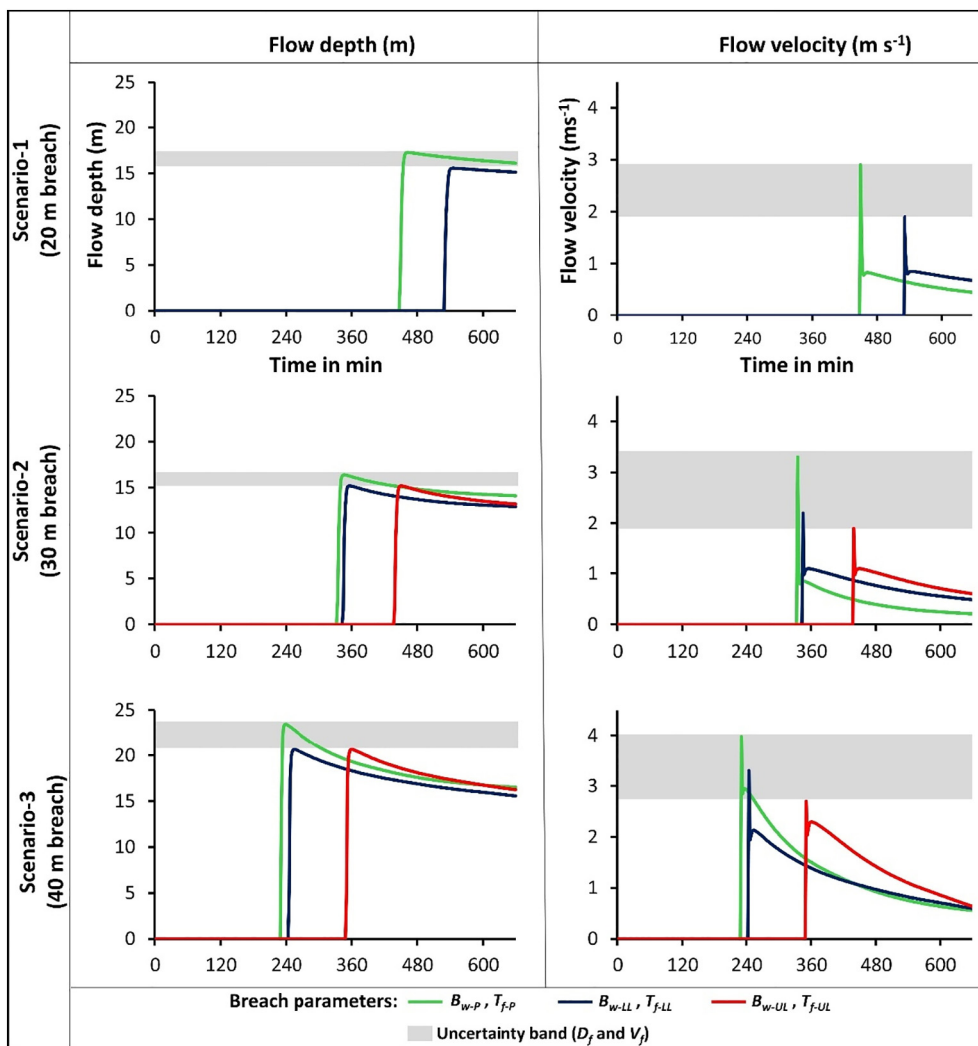


**Fig. 11.** Time series of flow depth and flow velocity at Chungthang for each predicted GLOF scenario; the time series is evaluated at a single point at Chungthang, the location of which is marked in Fig. 10A.

stagnant lake water, thereby creating an impulse wave (Worni et al., 2014; Byers et al., 2019). However, such impacts on the lake would be potentially dwarfed by any catastrophic ice/rock avalanches originating from the headwall behind the lake. To reach the current lake extent, such avalanches would need to obtain overall slope trajectory angles as low as  $14^\circ$ , making this a potentially feasible (see Schneider et al., 2011) low likelihood/ high impact scenario. Nonetheless, for the design of early warning systems and other risk reduction strategies, a full range of possible scenarios should be considered, including worst-case events. For example, the potential land area affected by such a worst-case event could be marked as an area of residual danger in a final hazard map, depending on local regulations and norms (NDMA, 2020).

The eventual magnitude of the impulse wave is dependent on the avalanche characteristics and morphology of the lake, which in turn determines the wave run-up height and overtopping (Schaub et al., 2016). In the case of South Lhonak Lake, the lake has a tapering downstream end and a 7 m high crest height above lake level in the front. Due to the spindle shape of the lake, the impulse-wave amplitudes can rise higher as it approaches the shore, potentially causing higher overtopping than calculated.

Based on the avalanche modeling and runout distances, it is seen that the avalanches reaching the future lake ( $S_{ava-3}$ ,  $S_{ava-4}$ ,  $S_{ava-5}$ , and  $S_{ava-6}$ ) can cause an impact before it is fully grown (see Fig. 7). In the future lake modeling, we see that the overdeepening extends up to 1.2 km

upstream from the current terminus (Fig. 5 and Fig. 6). For example, based on the runout of  $S_{ava-6}$ , it can cause an impact even when the lake grows up to 0.57 km from the current terminus (Fig. 7F). Similarly, scenarios  $S_{ava-5}$ ,  $S_{ava-4}$ , and  $S_{ava-3}$  can impact the lake when it grows to 0.60 km, 0.66 km, and 0.85 km upstream from the current terminus (Fig. 7C, D and E). However, it is to be noted that the severity/magnitude of any prior avalanche impact and overtopping event will be relatively lower than an impact on a fully-grown lake because (a) the total volume of the lake will be less than the fully-grown lake; and (b) the avalanche mass entering the lake will be comparably less as compared to the fully-grown lake, where the lake boundary is near to the avalanche source.

Apart from the potential slope movements, a lake (North Lhonak Lake) located upstream of the South Lhonak Lake may trigger cascading events in case of an outburst or overtopping (Fig. 1B). We note that there is a continuous discharge to the South Lhonak Lake along a narrow channel that originates from the North Lhonak Lake. In the case of rapid inflow, this could lead to overfilling of South Lhonak lake resulting in increased hydrostatic pressure on the damming moraine. Such process chains involving several lakes reveal that downstream lakes may have a mitigation or amplification role in the process chain propagation (e.g., Emmer, 2017; Mergili et al., 2018a, 2018b; or Kirschbaum et al., 2019).

The prediction of breach depth for potential GLOFs is uncertain. Therefore, we consider three potential GLOF originating from the lake

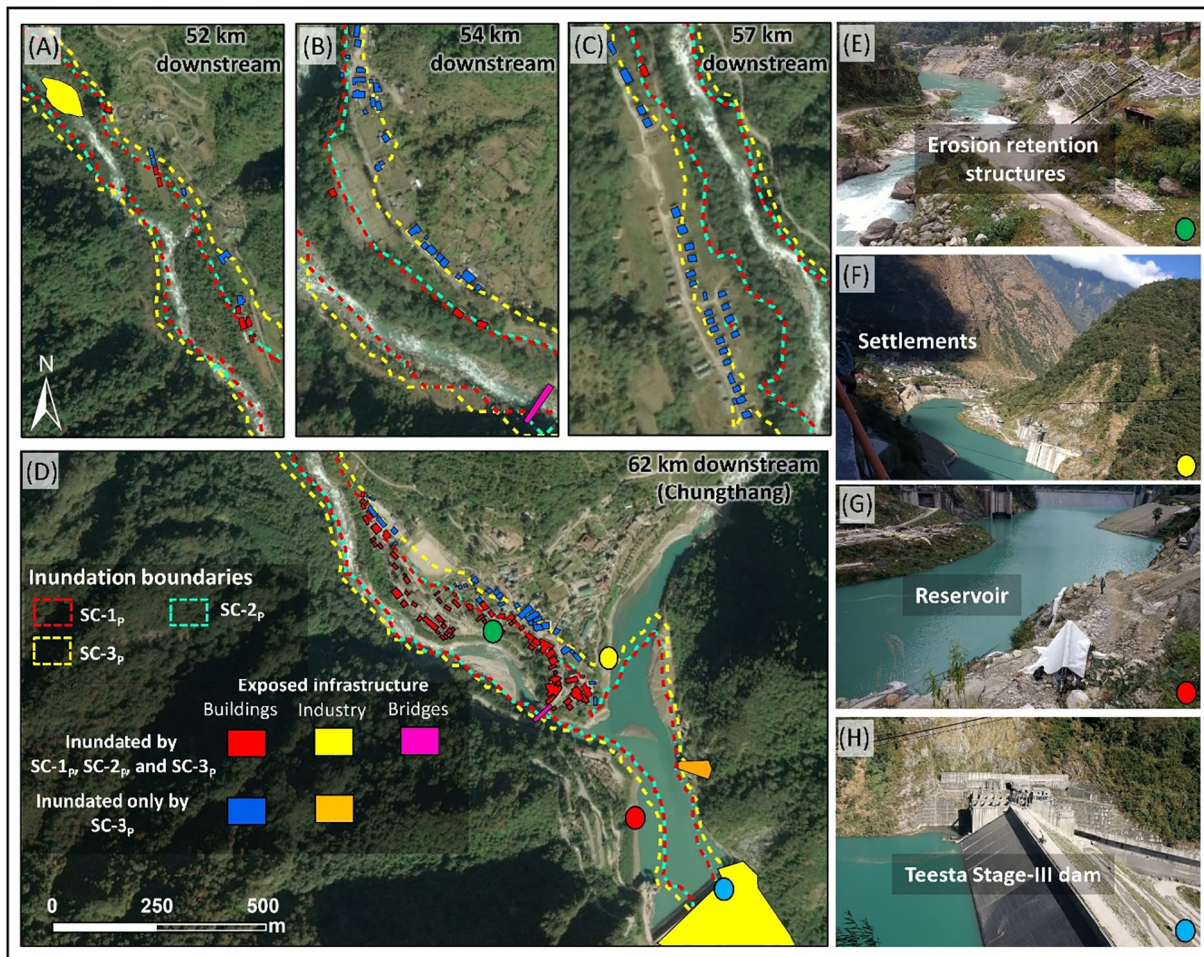


**Fig. 12.** (A-D) Mapped “at-risk” infrastructure along the flow channel for each predicted GLOF scenario; Google Earth imagery in the background; (E-H) Field photographs at different locations (the colored dots represent the respective locations marked in panel D).

of different magnitudes as low, moderate, and large. Due to the unavailability of any geophysical data of the frontal moraine, we modeled GLOFs where the breach depth reaches upto 40 m based on the moraine geometry. Here, the breach (40 m) in a large-potential GLOF is higher than the previously considered breach depths of 15 m for a potential current GLOF (Sattar et al., 2019a). Assuming that greater lake volume in the future can lead to increased hydrostatic pressure on the moraine, we evaluate GLOF's higher down-cutting of the frontal moraine during a

breaching event. The arrival timing in the present study is significantly delayed downstream of Lachen compared to Sattar et al. (2019a), possibly due to better representation of Mannings' roughness coefficient. Here, we note the importance of spatially distributed Manning's roughness in GLOF modeling because it can greatly influence GLOF hydraulics, especially its arrival timing and flow velocity. In the present study, a spatially distributed channel roughness was considered to account for the different LULC classes along the channel. Downstream of Lachen,

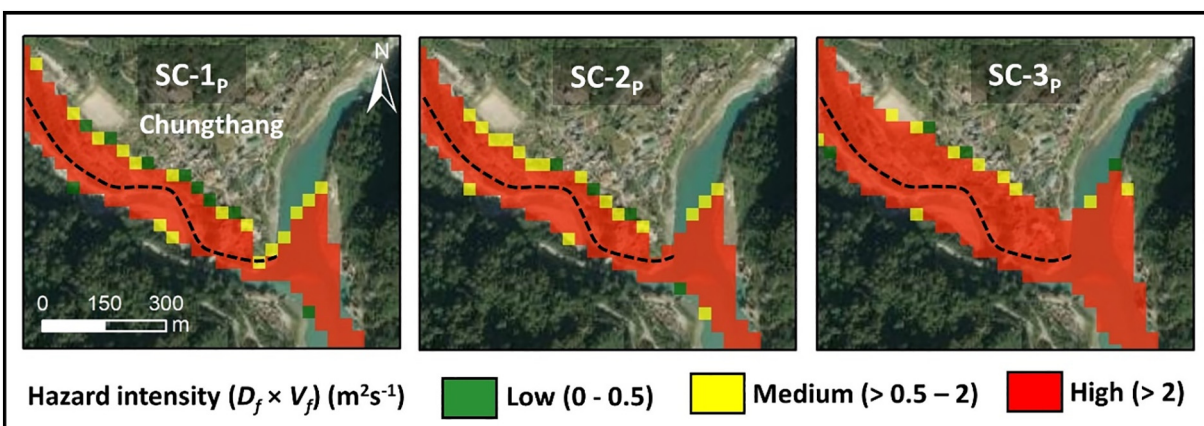


**Fig. 13.** Hazard intensity map of Chungthang based on flow heights (m) and velocity ( $m s^{-1}$ ) of each predicted GLOF scenario; black dotted line demarcates the shoreline.



**Fig. 14.** Evolution of the Chungthang town. The rapid growth of the infrastructure is seen after the establishment of the hydropower setup.

where vegetation cover is present, this led to attenuation of the flow velocity compared to the uniform channel roughness value considered in Sattar et al. (2019a).

We evaluated the flow hydraulics of water-only flow. Due to model limitations, the study does not account for the suspended debris, erosion, and deposition processes commonly associated with an outburst from moraine-dammed lakes (e.g., Worni et al., 2012). However, we recognize the scope of debris transport modeling in this case. The overtopping hazard in the valley is minimum for the scenarios

considered here, assuming no erosion of the damming moraine. The flow from overtopping even under the largest scenario (resulting from the impact of  $S_{ava}-6$ ), terminates at approximately 13 km downstream of the lake, i.e., 33 km upstream of Lachen. The valley is currently devoid of any infrastructure in the higher reaches.

#### 5.1.2. Socio-economical drivers of GLOF exposure and vulnerability

The South Lhonak valley population was under moderate growth even before the new hydropower construction, but the demand for

energy, suitable headwater, and stable discharge throughout the year has attracted large investments in hydropower sites and a rapid move towards regional urbanization. The construction of the Hydropower plant at Chungthang has recently been completed. It has increased the chances of continuous availability of power in the region and possible growth of more small-scale industries. The hydropower plant is expected to foster economic development in the region; however, as reflected in the recent constructions, it could also lead to building houses and other facilities on slopes closer to the river valley, thus increasing the risk. The increasing infrastructure in the region is leading to loss of vegetated river banks, reducing this natural buffer to flooding. This trend is common across the HKKH, where poorly regulated expansion of housing, roads, tourism, and other related infrastructure increases the risk to GLOFs and other disasters (Ziegler et al., 2014; Sati et al., 2011).

These observations reinforce that both socio-economic and natural drivers control GLOF risk. In other words, on the one hand, climate-driven growth of South Lhonak Lake increases the potential flood volume, while areal lake expansion towards steep slopes increases the likelihood of the lake being struck by a mass movement. On the other hand, socio-economic development as illustrated for Chungthang, and related changes in potentially flooded areas (population growth, urbanization, and road construction efforts) increase exposure to GLOF hazard. Complicating the situation further, socio-economic development can conversely increase the connectivity, livelihood, and perspectives for previously isolated rural communities, decreasing their vulnerability (Sidle and Ziegler, 2012). This comprehensive perspective on diverse drivers of GLOF risk in this region highlights the need for a shift from predominantly hazard-oriented studies to integrated studies that addresses all 3 drivers of GLOF risk. It is clear that for sustainable development, a concerted effort is required to balance economic growth in the region and avoid unnecessary construction in the path of potential GLOF and other natural hazards.

## 5.2. Uncertainty in GLOF modeling and future work recommendations

Dam-break assessment can be greatly influenced by the input breach parameters, which determine the magnitude of flow hydraulics downstream of the breaching site. The present study shows that the outflow hydraulics are highly sensitive to the breach formation time ( $T_f$ ). Several previous dam-break assessments also reported outflow discharge to be highly sensitive to  $T_f$  (Singh and Snorrason, 1982; Basheer et al., 2017; Sattar et al., 2020). Higher  $T_f$  produces lower peak discharge where the time taken to reach the peak is delayed even when the  $B_w$  and PFV are kept constant and thus it influences the routed flow hydraulics downstream. In South Lhonak Lake, when the upper limit of breach parameters is considered, the time to reach the peak in a GLOF hydrograph is delayed by an average of 112 min, and the arrival time of the flood wave at Chungthang is delayed by 95 min. For disaster preparedness and setting up an early warning system, it is recommended to consider the shortest flood arrival time for evacuation purposes. In addition, the uncertainty in  $Q_{max}$  increases as the breach depth and PFV are higher (Fig. 9). The uncertainty in the arrival remains more or less constant at locations downstream. Further, the uncertainty in the flow depths and velocity calculated at Chungthang shows that flow velocity ( $V_f$ ) is more sensitive than the flow depths ( $D_f$ ) (Fig. 11). Future efforts to assess GLOF risk in the valley can focus on a detailed field investigation of the flow channel to identify potential erosion and debris entrainment zones. Also, lake-lowering scenarios can be modeled to evaluate the change in the flow hydraulics downstream. With the current retreat rate of the South Lhonak glacier, it is recommended to regularly monitor the lakes' growth, the stability of surrounding slopes, and the state of the frontal moraine. For GLOF mitigation, modeling the effect of different mitigation strategies like check dams or levees can be evaluated before actual ground implementation. For higher-order precision of GLOF hydraulics, fine resolution elevation models are recommended.

## 6. Conclusions

Our study evaluates the future GLOF hazard of the largest proglacial lake in Sikkim, South Lhonak Lake. The future volume of the lake based on an ice-thickness approach is calculated to be  $114.8 \times 10^6 \text{ m}^3$ . This enormous volume of water in a highly dynamic high-mountain environment makes this lake a priority for GLOF risk management. Our results show that the GLOF susceptibility will increase due to the expansion of the lake towards steep slopes, which are considered potential starting zones of avalanches. These avalanches can create an impulse-wave when hitting the lake and are considered the most likely GLOF trigger for the South Lhonak Lake.

A number of GLOF scenarios were defined (both dam overtopping and breach), considering different avalanche scenarios (magnitudes). Modeling results conclude that dam overtopping would likely be attenuated several kilometers downstream from the lake due to moderate overtopping volume and gently sloped topography directly downstream of the lake, where the flow energy dissipates. Whereas the main hazard for downstream areas is associated with the potential dam breach events, that would result in far-reaching floods. Further, we demonstrated the effect of uncertainty of the breach parameters on breach simulations and its influence on the flow hydraulics downstream. More specifically our results show that the uncertainty in the breach parameters greatly influences GLOF arrival time and the hydraulic peaks at different locations. Hazard intensity mapping based on the GLOF scenarios considered in the study shows that many settlements along the valley, including the largest town Chungthang, are at high risk where both flow depth and velocity can reach up to 20–30 m and 6–9 m s<sup>-1</sup>, respectively. Due to the construction of the hydropower dam at Chungthang in 2015, GLOF risk mitigation in relation to South Lhonak and other critical lakes in the basin is of utmost importance. The results presented in the study can serve as base data, that could complement additional scenarios for GLOF risk management and the design of an early warning system in the valley.

## Declaration of competing interest

The authors declare no conflict of interest. The funders had no role in the design of the study; in the collection, analyses, or interpretation of data; in the writing of the manuscript, or in the decision to publish the results.

## Acknowledgments

We thank the associate editor and two anonymous reviewers for their insightful comments. The authors would like to acknowledge the Department of Geology and Environmental Geosciences, University of Dayton for providing necessary infrastructure and computational facilities. The authors would further like to acknowledge USGS, Digital Globe, and NavInfo for the remote sensing datasets employed in the study. We acknowledge the Department of Science and Technology, Government of Sikkim and Dr. Mona Chettri Post-Doctoral Research Fellow at the Australia-India Institute, University of Western Australia for the field photographs. We are very grateful for the support from various funding programs for the last several years. Specifically, the following grants made this work possible at different stages: MHRD, MoES, Project no. IMPRINT 4096 (to AG and AVK). UKH and AS was supported by the National Aeronautics and Space Administration (NASA) Interdisciplinary Research in Earth Science grant number 80NSSC18K0432. UKH was also supported by the NASA High Mountain Asia grant number 80NSSC19K0653 and NASA Cryosphere grant number 80NSSC20K1442. SA, HF, and CH are supported by the Swiss Agency for Development and Cooperation (SDC), in framework of the project Disaster Risk Management Planning and Implementation Support in the Indian Himalayan Region. AS acknowledges the Swiss Government Excellence Award for

funding and the Department of Geography, University of Zurich for necessary computational facilities.

## Appendix A. Supplementary data

Supplementary data to this article can be found online at <https://doi.org/10.1016/j.geomorph.2021.107783>.

## References

- Aggarwal, S., Rai, S.C., Thakur, P.K., Emmer, A., 2017. Inventory and recently increasing GLOF susceptibility of glacial lakes in Sikkim, Eastern Himalaya. *Geomorphology* 295, 39–54.
- Allen, S.K., Linsbauer, A., Randhawa, S.S., Huggel, C., Rana, P., Kumari, A., 2016. Glacial lake outburst flood risk in Himachal Pradesh, India: an integrative and anticipatory approach considering current and future threats. *Nat. Hazards* 84 (3), 1741–1763.
- Allen, S.K., Zhang, G., Wang, W., Yao, T., Bolch, T., 2019. Potentially dangerous glacial lakes across the Tibetan Plateau revealed using a large-scale automated assessment approach. *Science Bulletin* 64 (7), 435–445.
- Anaona, P.I., Mackintosh, A., Norton, K., 2015. Reconstruction of a glacial lake outburst flood (GLOF) in the Engaño Valley, Chilean Patagonia: Lessons for GLOF risk management. *Sci. Total Environ.* 527, 1–11.
- Azam, M.F., Wagnon, P., Berthier, E., Vincent, C., Fujita, K., Kargel, J.S., 2018. Review of the status and mass changes of Himalayan-Karakoram glaciers. *J. Glaciol.* 64 (243), 61–74.
- Bajracharya, S.R., Mool, P.K., Shrestha, B.R., 2008. Global climate change and melting of Himalayan glaciers. *Melting Glaciers and Rising Sea Levels: Impacts and Implications*, pp. 28–46.
- Bartelt, P., Salm, B., Gruber, U., 1999. Calculating dense-snow avalanche runout using a Voellmy-fluid model with active/passive longitudinal straining. *J. Glaciol.* 45 (150), 242–254.
- Bartelt, P., Buehler, Y., Christen, M., Deubelbeiss, Y., Graf, C., Mc Ardell, B., Sals, M., and Schneider, M.: RAMMS: Rapid Mass Movement Simulation: A numerical model for debris flows in research and practice, User Manual v1.5 – Debris Flow, Swiss Institute for Snow and Avalanche Research SLF, Birmensdorf, 2013.
- Basheer, T.A., Wayayok, A., Yusuf, B., KAMAL, M., 2017. Dam Breach parameters and their influence on flood hydrographs for Mosul Dam. *Journal of Engineering Science and Technology* 12 (11), 2896–2908.
- Bicherion, P., Defourny, P., Brockmann, C., Schouten, L., Vancutsem, C., Huc, M., Bontemps, S., Leroy, M., Achard, F., Herold, M., Ranera, F., 2008. *GLOBECOVER: Products Description and Validation Report*.
- Bolch, T., Kulkarni, A., Kääb, A., Huggel, C., Paul, F., Cogley, J.G., Frey, H., Kargel, J.S., Fujita, K., Scheel, M., Bajracharya, S., 2012. The state and fate of Himalayan glaciers. *Science* 336 (6079), 310–314.
- Byers, A.C., Rounce, D.R., Shugar, D.H., Lala, J.M., Byers, E.A., Regmi, D., 2019. A rockfall-induced glacial lake outburst flood, Upper Barun Valley, Nepal. *Landslides* 16 (3), 533–549.
- Byers, A.C., Chand, M.B., Lala, J., Shrestha, M., Byers, E.A., Watanabe, T., 2020. Reconstructing the history of Glacial Lake Outburst Floods (GLOF) in the Kanchenjunga Conservation Area, East Nepal: an interdisciplinary approach. *Sustainability* 12 (13), 5407.
- Carey, M., Huggel, C., Bury, J., Portocarrero, C., Haeberli, W., 2012. An integrated socio-environmental framework for glacier hazard management and climate change adaptation: lessons from Lake 513, Cordillera Blanca, Peru. *Clim. Chang.* 112 (3–4), 733–767.
- Christen, M., Kowalski, J., Bartelt, P., 2010. RAMMS: Numerical simulation of dense snow avalanches in three-dimensional terrain. *Cold Reg. Sci. Technol.* 63 (1–2), 1–14.
- Clague, J.J., Evans, S.G., 2000. A review of catastrophic drainage of moraine-dammed lakes in British Columbia. *Quat. Sci. Rev.* 19 (17–18), 1763–1783.
- Drenkhan, F., Huggel, C., Guardamino, L., Haeberli, W., 2019. Managing risks and future options from new lakes in the deglaciating Andes of Peru: the example of the Vilcanota-Urubamba basin. *Sci. Total Environ.* 665, 465–483.
- Dubey, S., Goyal, M.K., 2020. Glacial Lake Outburst Flood hazard, downstream impact, and risk over the Indian Himalayas. *Water Resour. Res.* 56 (4), e2019WR026533.
- Emmer, A., 2017. Geomorphologically effective floods from moraine-dammed lakes in the Cordillera Blanca, Peru. *Quat. Sci. Rev.* 177, 220–234.
- Emmer, A., 2018. GLOFs in the WOS: bibliometrics, geographies and global trends of research on glacial lake outburst floods (Web of Science, 1979–2016). *Nat. Hazards Earth Syst. Sci.* 18, 813–827.
- Emmer, A., Le Roy, M., Sattar, A., Veetil, B.K., Alcalá-Reygosa, Jesú, Campos, Né, Malecki, J., Cochachin, A., 2021. Glacier retreat and associated processes since the last glacial maximum in the lejiamayu valley, Peruvian Andes, *Journal of South American Earth Sciences* <https://doi.org/10.1016/j.jsames.2021.1032>.
- Evers, F., Heller, V., Fuchs, H., Hager, W.H., Boes, R., 2019. Landslide-generated Impulse Waves in Reservoirs: Basics and Computation. *VAW-Mitteilungen* 254.
- Farinotti, D., Brinkerhoff, D.J., Clarke, G.K., Fürst, J.J., Frey, H., Gantayat, P., Gillet-Chaulet, F., Girard, C., Huss, M., Leclercq, P.W., Linsbauer, A., 2017. How accurate are estimates of glacier ice thickness? Results from ITMIX, the Ice Thickness Models Intercomparison eXperiment. *Cryosphere* 11 (2), 949–970.
- Farinotti, D., Huss, M., Fürst, J.J., Landmann, J., Machguth, H., Maussion, F., Pandit, A., 2019. A consensus estimate for the ice thickness distribution of all glaciers on Earth. *Nat. Geosci.* 12 (3), 168–173.
- Farinotti, D., Immerzeel, W.W., de Kok, R.J., Quincey, D.J., Dehecq, A., 2020. Manifestations and mechanisms of the Karakoram glacier Anomaly. *Nat. Geosci.* 13 (1), 8–16.
- Frey, H., Machguth, H., Huss, M., Huggel, C., Bajracharya, S., Bolch, T., Kulkarni, A., Linsbauer, A., Salzmann, N., Stoffel, M., 2014. Estimating the volume of glaciers in the Himalayan–Karakoram region using different methods. *Cryosphere* 8 (6), 2313–2333.
- Frey, H., Huggel, C., Chisolm, R.E., Baer, P., Mc Ardell, B., Cochachin, A., Portocarrero, C., 2018. Multi-source glacial lake outburst flood hazard assessment and mapping for Huánuco, Cordillera Blanca, Peru. *Front. Earth Sci.* 6, 210.
- Froehlich, D.C., 1995a. Peak Outflow from Breached Embankment Dam. *J. Water Resour. Plan. Manag.* 121 (1), 90–97.
- Froehlich, D.C., 1995b. "Embankment Dam Breach Parameters Revisited," Water Resources Engineering, Proceedings of the 1995 ASCE Conference on Water Resources Engineering, San Antonio, Texas, August 14–18, 1995, p. 887–891. American Society of Civil Engineers, Reston, VA.
- Fujita, K., Sakai, A., Takenaka, S., Nuimura, T., Surazakov, A.B., Sawagaki, T., Yamanokuchi, T., 2013. Potential flood volume of Himalayan glacial lakes. *Natural Hazards & Earth System Sciences* 13 (7).
- Fürst, J.J., Gillet-Chaulet, F., Benham, T., Dowdeswell, J., Grabiec, M., Navarro, F., Pettersson, R., Moholdt, G., Nuth, C., Sass, B., Aas, K., 2017. Application of a Two-step Approach for Mapping Ice Thickness to Various Glacier Types on Svalbard.
- GAPHAZ, 2017. Assessment of Glacier and Permafrost Hazards in Mountain Regions – Technical Guidance Document. Prepared by Allen S, Frey H, Huggel C. et al. Standing Group on Glacier and Permafrost Hazards in Mountains (GAPHAZ) of the International Association of Cryospheric Sciences (IACS) and the International Permafrost Association (IPA).
- Gardelle, J., Arnaud, Y., Berthier, E., 2011. Contrasted evolution of glacial lakes along the Hindu Kush Himalaya mountain range between 1990 and 2009. *Glob. Planet. Chang.* 75 (1–2), 47–55.
- Haeberli, W., Buettner, M., Huggel, C., Friedli, T.L., Schaub, Y., Schleiss, A.J., 2016. New lakes in deglaciating high-mountain regions—opportunities and risks. *Clim. Chang.* 139 (2), 201–214.
- Haeberli, W., Schaub, Y., Huggel, C., 2017. Increasing risks related to landslides from degrading permafrost into new lakes in de-glaciating mountain ranges. *Geomorphology* 293, 405–417.
- Haritashya, U.K., Kargel, J.S., Shugar, D.H., Leonard, G.J., Stratton, K., Watson, C.S., Shean, D., Harrison, S., Mandli, K.T. and Regmi, D., 2018. Evolution and controls of large glacial lakes in the Nepal Himalaya. *Remote Sensing*, 10(5), p.798.
- Heller, V., Hager, W.H., Minor, H.-E., 2009. Landslide Generated Impulse Waves in Reservoirs. *Zürich: Mitteilungen Versuchsanstalt für Wasserbau, ETH Zürich, Hydrologie und Glaziologie (VAW)*.
- Hock, R., Rasul, G., Adler, C., Cáceres, B., Gruber, S., Hirabayashi, Y., Jackson, M., Kääb, A., Kang, S., Kutuzov, S., Milner, A., 2019. High Mountain Areas: In: IPCC Special Report on the Ocean and Cryosphere in a Changing Climate.
- Hoelzle, M., Haeberli, W., Disch, M., Peschke, W., 2003. Secular glacier mass balances derived from cumulative glacier length changes. *Glob. Planet. Chang.* 36 (4), 295–306.
- Huggel, C., Haeberli, W., Kääb, A., Bieri, D., Richardson, S., 2004. An assessment procedure for glacial hazards in the Swiss Alps. *Can. Geotech. J.* 41 (6), 1068–1083.
- Huggel, C., Carey, M., Emmer, A., Frey, H., Walker-Crawford, N., Wallmann-Helmer, I., 2020. Anthropogenic climate change and glacier lake outburst flood risk: local and global drivers and responsibilities for the case of lake Palcacocha, Peru. *Nat. Hazards Earth Syst. Sci.* 20 (8), 2175–2193.
- Huss, M., Farinotti, D., 2012. Distributed ice thickness and volume of all glaciers around the globe. *Journal of Geophysical Research: Earth Surface* 117 (F4).
- Kargel, J.S., Leonard, G.J., Shugar, D.H., Haritashya, U.K., Bevington, A., Fielding, E.J., Fujita, K., Geertsema, M., Miles, E.S., Steiner, J., Anderson, E., 2016. Geomorphic and geologic controls of geohazards induced by Nepal's 2015 Gorkha earthquake. *Science* 351 (6269).
- King, O., Bhattacharya, A., Bhambri, R., Bolch, T., 2019. Glacial lakes exacerbate Himalayan glacier mass loss. *Sci. Rep.* 9 (1), 1–9.
- Kirschbaum, D., Watson, C.S., Rounce, D.R., Shugar, D., Kargel, J.S., Haritashya, U.K., Amatya, P., Shean, D., Anderson, E.R., Jo, M., 2019. The State of Remote Sensing Capabilities of Cascading Hazards Over High Mountain Asia. *Front. Earth Sci.* 7, 197.
- Klimeš, J., Novotný, J., Novotná, I., de Urries, B.J., Vilímek, V., Emmer, A., Strozzi, T., Kusák, M., Rapre, A.C., Hartvich, F., Frey, H., 2016. Landslides in moraines as triggers of glacial lake outburst floods: example from Palcacocha Lake (Cordillera Blanca, Peru). *Landslides* 13 (6), 1461–1477.
- Komori, J., 2008. Recent expansions of glacial lakes in the Bhutan Himalayas. *Quat. Int.* 184 (1), 177–186.
- Korup, O., Tweed, F., 2007. Ice, moraine, and landslide dams in mountainous terrain. *Quat. Sci. Rev.* 26 (25–28), 3406–3422.
- Kougkoulos, I., Cook, S.J., Edwards, L.A., Clarke, L.J., Symeonakis, E., Dorch, J.M., Nesbitt, K., 2018. Modelling glacial lake outburst flood impacts in the Bolivian Andes. *Nat. Hazards Earth Syst. Sci.* 94 (3), 1415–1438.
- Kumar, B., Murugesh Prabhu, T.S., 2012. Impacts of climate change: glacial lake outburst floods (GLOFs). *Climate Change in Sikkim Patterns*. Information and Public Relations Department, Government of Sikkim, Gangtok, Impacts and Initiatives.
- Lala, J.M., Rounce, D.R., McKinney, D.C., 2018. Modeling the glacial lake outburst flood process chain in the Nepal Himalaya: reassessing Imja Tsho's hazard. *Hydrol. Earth Syst. Sci.* 22 (7), 3721–3737.
- Linsbauer, A., Paul, F., Haeberli, W., 2012. Modeling glacier thickness distribution and bed topography over entire mountain ranges with GladTop: application of a fast and robust approach. *Journal of Geophysical Research: Earth Surface* 117 (F3).
- Linsbauer, A., Frey, H., Haeberli, W., Machguth, H., Azam, M.F., Allen, S., 2016. Modelling glacier-bed overdeepenings and possible future lakes for the glaciers in the Himalaya–Karakoram region. *Ann. Glaciol.* 57 (71), 119–130.
- Liu, J.J., Tang, C., Cheng, Z.L., 2013. The two main mechanisms of glacier lake outburst flood in Tibet, China. *J. Mt. Sci.* 10 (2), 239–248.

- Majeed, U., Rashid, I., Sattar, A., Allen, S., Stoffel, M., Nüsser, M., Schmidt, S., 2021. Recession of Gya Glacier and the 2014 glacial lake outburst flood in the Trans-Himalayan region of Ladakh, India. *Sci. Total Environ.* 756, 144008.
- Maussion, F., Butenko, A., Eis, J., Fourteau, K., Jarosch, A.H., Landmann, J., Oesterle, F., Recinos, B., Rothenpieler, T., Vlug, A., Wild, C.T., 2018. The Open Global Glacier Model (OGGM) v1.0. *Geosci. Dev. Discuss. Model.*
- Mergili, M., Emmer, A., Juřicová, Á., Cochachin, A., Fischer, J.T., Huggel, C., Pudasaini, S.P., 2018a. How well can we simulate complex hydro-geomorphic process chains? The 2012 multi-lake outburst flood in the Santa Cruz Valley (Cordillera Blanca, Perú). *Earth Surf. Process. Landf.* 43 (7), 1373–1389.
- Mergili, M., Frank, B., Fischer, J.T., Huggel, C., Pudasaini, S.P., 2018b. Computational experiments on the 1962 and 1970 landslide events at Huascarán (Peru) with r. avaflow: lessons learned for predictive mass flow simulations. *Geomorphology* 322, 15–28.
- Mool, P.K., Bajracharya, S.R., Shrestha, B., Joshi, S.P., Roohi, R., Ashraf, A., Naz, R., Hussain, S.A. and Chaudhry, M.H., 2003. Inventory of Glaciers, Glacial Lakes and the Identification of Potential Glacial Lake Outburst Floods (GLOFs) Affected by Global Warming in the Mountains of Himalayan Region: Tista Basin, Sikkim Himalaya, India. Unpublished project report, with database on CD-ROM, prepared for APN and ICIMOD, Kathmandu.
- NDMA 2020: National Disaster Management Authority Guidelines Management of Glacial Lake Outburst Floods (GLOFs), Delhi, India 113 pp.
- Osti, R., Egashira, S., 2009. Hydrodynamic characteristics of the Tam Pokhari Glacial Lake outburst flood in the Mt. Everest region. *Nepal. Hydrological Processes: An International Journal* 23 (20), 2943–2955.
- Paterson, W.S.B., 1994. Physics of glaciers. Butterworth-Heinemann.
- Paul, F., Kähäri, A., Maisch, M., Kellenberger, T., Haeberli, W., 2004. Rapid disintegration of Alpine glaciers observed with satellite data. *Geophys. Res. Lett.* 31 (21).
- Raj, K.B.G., Kumar, V.K., 2016. Inventory of glacial lakes and its evolution in Uttarakhand Himalaya using time series satellite data. *Journal of the Indian Society of Remote Sensing* 44 (6), 959–976.
- Raj, K.B.G., Kumar, V.K., SN, R., 2013. Remote sensing-based inventory of glacial lakes in Sikkim Himalaya: semi-automated approach using satellite data. *Geomatics, Natural Hazards and Risk* 4 (3), 241–253.
- Ray, P.C., Chattoraj, S.L., Bisht, M.P.S., Kannaujiya, S., Pandey, K., Goswami, A., 2016. Kedarnath disaster 2013: causes and consequences using remote sensing inputs. *Nat. Hazards* 81 (1), 227–243.
- Richardson, S.D., Reynolds, J.M., 2000. An overview of glacial hazards in the Himalayas. *Quat. Int.* 65, 31–47.
- Rounce, D.R., McKinney, D.C., Lala, J.M., Byers, A.C., Watson, C.S., 2016. A new remote hazard and risk assessment framework for glacial lakes in the Nepal Himalaya. *Hydrol. Earth Syst. Sci.* 20, 3455–3475.
- Sati, S.P., Sundriyal, Y.P., Rana, N., Dangwal, S., 2011. Recent landslides in Uttarakhand: nature's fury or human folly. *Current Science(Bangalore)* 100 (11), 1617–1620.
- Sattar, A., Goswami, A., Kulkarni, A.V., 2019a. Hydrodynamic moraine-breach modeling and outburst flood routing—a hazard assessment of the South Lhonak lake, Sikkim. *Sci. Total Environ.* 668, 362–378.
- Sattar, A., Goswami, A., Kulkarni, A.V., Das, P., 2019b. Glacier-surface velocity derived ice volume and retreat assessment in the Dhauliganga basin, Central Himalaya—a remote sensing and modeling based approach. *Front. Earth Sci.* 7, 105.
- Sattar, A., Goswami, A., Kulkarni, A.V., 2019c. Application of 1D and 2D hydrodynamic modeling to study glacial lake outburst flood (GLOF) and its impact on a hydropower station in Central Himalaya. *Nat. Hazards* 97 (2), 535–553.
- Sattar, A., Goswami, A., Kulkarni, A., Emmer, A., 2020. Lake evolution, hydrodynamic outburst flood modeling and sensitivity analysis in the central Himalaya: a case study. *Water* 12 (1), 237.
- Schaub, Y., Huggel, C., Cochachin, A., 2016. Ice-avalanche scenario elaboration and uncertainty propagation in numerical simulation of rock-/ice-avalanche-induced impact waves at Mount Hualcán and Lake 513, Peru. *Landslides* 13 (6), 1445–1459.
- Schneider, D., Bartelt, P., Caplan-Auerbach, J., Christen, M., Huggel, C., McArdell, B.W., 2010. Insights into rock-ice avalanche dynamics by combined analysis of seismic recordings and a numerical avalanche model. *Journal of Geophysical Research: Earth Surface* 115 (F4).
- Schneider, D., Huggel, C., Haeberli, W., Kaitna, R., 2011. Unraveling driving factors for large rock-ice avalanche mobility. *Earth Surf. Process. Landf.* 36 (14), 1948–1966.
- Schneider, D., Huggel, C., Cochachin, A., Guillén, S., García, J., 2014. Mapping hazards from glacier lake outburst floods based on modelling of process cascades at Lake 513, Carhuaz, Peru. *Adv. Geosci.* 35, 145–155.
- Sharma, R.K., Pradhan, P., Sharma, N.P., Shrestha, D.G., 2018. Remote sensing and in situ-based assessment of rapidly growing South Lhonak glacial lake in eastern Himalaya, India. *Nat. Hazards* 93 (1), 393–409.
- Shugar, D.H., Burr, A., Haritashya, U.K., Kargel, J.S., Watson, C.S., Kennedy, M.C., Bevington, A.R., Betts, R.A., Harrison, S., Stratman, K., 2020. Rapid worldwide growth of glacial lakes since 1990. *Nature Climate Change*, pp. 1–7.
- Shukla, A., Garg, P.K., Srivastava, S., 2018. Evolution of glacial and high-altitude lakes in the Sikkim, Eastern Himalaya over the past four decades (1975–2017). *Frontiers in Environmental Science* 6, 81.
- Sidle, R.C., Ziegler, A.D., 2012. The dilemma of mountain roads. *Nat. Geosci.* 5 (7), 437–438.
- Singh, K.P., Snorrason, A., 1982. Sensitivity of Outflow Peaks and Flood Stages to the Selection of Dam Breach Parameters and Simulation Models (Dam Safety Program) (Illinois State Water Survey).
- Somos-Valenzuela, M.A., McKinney, D.C., Byers, A.C., Rounce, D.R., Portocarrero, C., Lamsal, D., 2015. Assessing downstream flood impacts due to a potential GLOF from Imja Tsho in Nepal. *Hydrology & Earth System Sciences* 19 (3).
- Somos-Valenzuela, M.A., Chisolm, R.E., Rivas, D.S., Portocarrero, C. and McKinney, D.C., 2016. Modeling a glacial lake outburst flood process chain: the case of Lake Palcacocha and Huaraz, Peru. *Hydrology and Earth System Sciences*, 20(6), p.2519.
- Sosio, R., Crosta, G.B., Hungr, O., 2008. Completed dynamic modeling calibration for the Thürwieser rock avalanche (Italian Central Alps). *Eng. Geol.* 100 (1–2), 11–26.
- Veh, G., Korup, O., von Specht, S., Roessner, S., Walz, A., 2019. Unchanged frequency of moraine-dammed glacial lake outburst floods in the Himalaya. *Nat. Clim. Chang.* 9 (5), 379–383.
- Vuichard, D. and Zimmermann, M., 1987. The 1985 catastrophic drainage of a moraine-dammed lake, Khumbu Himal, Nepal: cause and consequences. *Mountain Research and Development*, pp.91–110.
- Wahl, T.L., 1998. Prediction of Embankment Dam Breach Parameters - A Literature Review and Needs Assessment. U.S. Dept. of the Interior, Bureau of Reclamation, Dam Safety Report DSO-98-004, Denver, CO.
- Wahl, T.L., 2004. Uncertainty of predictions for Embankment Dam breach Parameters. *J. Hydraul. Eng.* 130, 389–397.
- Wan, C.F., Fell, R., 2004. Investigation of rate of erosion of soils in embankment dams. *J. Geotech. Geoenviron.* 130 (4), 373–380.
- Wang, W., Yang, X., Yao, T., 2012. Evaluation of ASTER GDEM and SRTM and their suitability in hydraulic modelling of a glacial lake outburst flood in southeast Tibet. *Hydrol. Process.* 26 (2), 213–225.
- Wang, W., Gao, Y., Anacona, P.I., Lei, Y., Xiang, Y., Zhang, G., Li, S., Lu, A., 2018. Integrated hazard assessment of Cirenmaco glacial lake in Zhangzangbo valley, Central Himalayas. *Geomorphology* 306, 292–305.
- Watanabe, T., Lamsal, D., Ives, J.D., 2009. Evaluating the growth characteristics of a glacial lake and its degree of danger of outburst flooding: Imja Glacier, Khumbu Himal, Nepal. *Norsk Geografisk Tidsskrift-Norwegian Journal of Geography* 63 (4), 255–267.
- Westoby, M.J., Glasser, N.F., Brasington, J., Hambrey, M.J., Quincey, D.J., Reynolds, J.M., 2014. Modelling outburst floods from moraine-dammed glacial lakes. *Earth Sci. Rev.* 134, 137–159.
- Worni, R., Stoffel, M., Huggel, C., Volz, C., Casteller, A., Luckman, B., 2012. Analysis and dynamic modeling of a moraine failure and glacier lake outburst flood at Ventisquero Negro, Patagonian Andes (Argentina). *J. Hydrol.* 444, 134–145.
- Worni, R., Huggel, C., Stoffel, M., 2013. Glacial lakes in the Indian Himalayas—from an area-wide glacial lake inventory to on-site and modeling based risk assessment of critical glacial lakes. *Sci. Total Environ.* 468, S71–S84.
- Worni, R., Huggel, C., Clague, J.J., Schaub, Y., Stoffel, M., 2014. Coupling glacial lake impact, dam breach, and flood processes: A modeling perspective. *Geomorphology* 224, 161–176.
- Zhang, G., Yao, T., Xie, H., Wang, W., Yang, W., 2015. An inventory of glacial lakes in the Third Pole region and their changes in response to global warming. *Glob. Planet. Chang.* 131, 148–157.
- Zheng, G., Bao, A., Allen, S., Antonio Ballesteros-Cánovas, J., Yuan, Y., Jiapaer, G., Stoffel, M., 2021. Numerous unreported glacial lake outburst floods in the Third Pole revealed by high-resolution satellite data and geomorphological evidence. *Science Bulletin*. <https://doi.org/10.1016/j.scib.2021.01.014>.
- Ziegler, A.D., Wasson, R.J., Bhardwaj, A., Sundriyal, Y.P., Sati, S.P., Juyal, N., Nautiyal, V., Srivastava, P., Gillen, J., Saklani, U., 2014. Pilgrims, progress, and the political economy of disaster preparedness—the example of the 2013 Uttarakhand flood and Kedarnath disaster. *Hydrol. Process.* 28 (24), 5985–5990.